3-12-2013

Influence of moving load, structure, temperature gradient, and wheel configuration on load transfer efficiency

Akshay Joshi

INFLUENCE OF MOVING LOAD, STRUCTURE, TEMPERATURE GRADIENT, AND WHEEL CONFIGURATION ON LOAD TRANSFER EFFICIENCY

by

Akshay Pradyumna Joshi

A Thesis

Submitted to the

Department of Civil Engineering

College of Engineering

In partial fulfillment of the requirement

For the degree of

Master of Science in Engineering

at

Rowan University

September 12, 2012

Thesis Chair: Yusuf Mehta, Ph.D., P.E.

Dedication

I would like to dedicate this manuscript to my parents, professors and friends

Acknowledgements

I would like to express my deepest gratitude to my Thesis Chair, Dr. Yusuf Mehta, whose diligence, zeal, and academic expertise inspired me to apply my skills to the fullest. His guidance throughout this research has been invaluable to me. I am extremely grateful to my Thesis co-Chair, Dr. Douglas Cleary, for sharing his expertise and providing encouraging and constructive feedback. He has always been inspirational, supportive, and patient throughout this research. Without the guidance and persistent help of my Thesis Chair and co-Chair this research would not have been possible.

I would like to convey my gratitude to Dr. David Brill from the Federal Aviation Administration (FAA) for his continual support, peerless feedback and determined effort in making all the resources in terms of data and software programs available for this research. In addition I would like to thank Dr. Gordon Hayhoe from FAA for serving on my thesis committee and the support and appreciation in carrying out this research at Rowan University. I would also like to thank Dr. Qiang Wang from SRA International for his efforts in making us fully acquainted with the software programs and relentlessly helping us in case of any queries.

I am also indebted to my colleagues in Civil & Environmental Engineering department at Rowan University who assisted me in this research. I owe my deepest admiration to Ashish Wadkar, Charles Cunliffe, Samuel Henry, Jeremy Soto, William McNally, Charles Calimer, Nicole Giannelli, Victor Smith and Harold Koenig for their effort and dedicated help in this research.

Abstract

Akshay Joshi

INFLUENCE OF MOVING LOAD, STRUCTURE, TEMPERATURE GRADIENT, AND WHEEL CONFIGURATION ON LOAD TRANSFER EFFICIENCY

2011/12

Yusuf Mehta, Ph.D., P.E.

Master of Science in Civil Engineering

An airport pavement consists of one or more paving materials over the natural subgrade. Pavement design involves the interaction of pavement with vehicular loads and climatic conditions. The Federal Aviation Administration (FAA) uses a mechanistic design procedure, FAARFIELD, for the design of rigid airport pavements. The FAARFIELD (**FAA R**igid and **F**lexible **I**terative **E**lastic **L**ayer **D**esign) procedure is based on layered elastic and three-dimensional finite element-based structural analysis developed to calculate design thicknesses for airfield pavements.

The design procedure assumes constant stress-based load transfer efficiency (LTE (S)), of 25% at the joints. Variations in environmental conditions, loading characteristics, type of joint and pavement material properties can affect load transfer efficiency. FAARFIELD does not consider curling stresses in determining the Portland Cement Concrete (PCC) layer thickness. The curling stresses, induced due to the temperature differentials at the top and bottom of the PCC slab can lead to higher combined stresses (loading plus curling) in pavements and can affect the load transfer efficiency at the joint. This study analyzes the effect of pavement layer properties, loading characteristics and temperature curling on stress-based load transfer efficiency. This study is carried out for static

loading conditions using FEAFAA (**F**inite **E**lement **A**nalysis – **FAA**) program. Results of this research indicate that LTE (S) is insensitive to modulus of PCC and base material. However, LTE (S) increases at negative temperature gradients (temperature at top of PCC surface > temperature at bottom of PCC) and when number of loaded areas (tire footprints) increase. It is observed that LTE (S) is highly sensitive to the joint stiffness including spacing of the dowel bars.

The airport pavement design procedure uses finite element models that are developed based on static analysis assuming that the speed of the vehicle is zero. However, most of the time, load transfer takes place under moving vehicles. Recently completed studies have shown that LTE (S) values under moving aircraft loads can be significantly higher than 0.25. This research documents a study of dynamic mechanical responses of rigid pavement at the joint under moving aircraft loads. The MRC (pavement constructed on conventional base) section of CC-2 (Construction Cycle–2) test pavement at the Federal Aviation Administration's (FAA) National Airport Pavement Test Facility (NAPTF) is modeled using 3D finite element software, ABAQUS. The model is calibrated by determining pavement damping parameters and joint stiffness values using heavy weight deflectometer (HWD) data and the strain profiles captured from the dynamic sensors installed within the pavement at various locations. The effect of moving aircraft at varying speeds on tensile strains at the bottom of PCC at the joint ($\varepsilon_{critical}$) and dynamic LTE (S) at the joint is studied. Results of this research indicate that $\varepsilon_{critical}$ at the joint decreases with increasing speed. The dynamic LTE (S) at the joint is enhanced at higher speeds. Sensitivity of dynamic LTE (S) to pavement damping showed that the dynamic LTE (S) at the joint increases with pavement damping.

Table of Contents

List of tables

List of figures

Chapter 1

Introduction

1.1 Rigid airport pavements

The function of airport pavements is to provide a firm support to satisfactorily accommodate trafficking aircraft loads throughout its operational life. Airport pavement design procedures are developed so as to fulfill the above criteria (AC 150/5320-6E, 2009). Various combinations of pavement types and stabilized layers result in complex pavement classification such as flexible, rigid, hot mix asphalt overlays, and rigid overlays. The analysis presented in this thesis is limited to rigid airfield pavements.

Almost all rigid pavements are made up of Portland Cement Concrete (PCC), typically consisting of PCC surface course constructed over either the subgrade or base course over subgrade. The PCC course is the stiffest and provides majority of strength to the pavement. The base course and the subgrade provide drainage and frost protection to the pavement and also contribute to the strength (http://training.ce.washington.edu/wsdot/, January 2011). Rigid pavements can be classified into three major categories:

a) Jointed plain concrete pavement (JPCP): In JPCP, the pavement is divided into individual slabs separated by contraction joints using dowels (for load transfer) and tie bars to connect adjacent slabs. This is the most common type of rigid pavement.

b) Jointed reinforced concrete pavement (JRCP): This type of pavement is similar to JPCP except that these slabs are much longer and are reinforced to withstand expansion and contraction due to temperature and moisture. The JRCP type is associated with long term performance problems and is not commonly used in the US.

c) Continuously reinforced concrete pavement (CRCP): In this type of rigid pavement the slabs are reinforced and continuous without any joints except construction joints.

Load Transfer:

Load transfer is used to describe the "transfer or distribution of load across discontinuities such as joints or cracks" (AASHTO, 1962). Load transfer across transverse joints/cracks is generally accomplished using one of the following (http://training.ce.washington.edu/wsdot/, January 2011):

a) Aggregate interlock: Load is transferred through mechanical interlocking of the aggregates across the joint. Load transfer through this mechanism can be typically used only for low-volume traffic.
b) Dowel bars: Dowels are short steel bars connecting adjacent slabs used to provide load transfer across the slabs. In this system, the load is transferred from the approach (loaded) slab to the leave (unloaded) slab through dowels thus reducing the stresses and deflections in the approach slab.
c) Reinforcing steel: In CRCP pavements, load is transferred across the cracks through the reinforcing steel.

Load Transfer efficiency (LTE): The stresses, strains and deflections in the loaded slab induced due to traffic loading are partly transferred to the unloaded slab through a combination of mechanisms mentioned above. The degree of load transfer or the load transfer efficiency (LTE) is generally defined based on transferred stresses / strains and deflections (Wadkar, 2010). Stress based load transfer efficiency (LTE (S)) is defined as the magnitude of free-edge stress or strain transferred to the unloaded slab and can be represented using equation 1.

$$LTE(S) = \frac{\sigma_{unloaded}}{(\sigma_{loaded}+\sigma_{unloaded})} = \frac{\varepsilon_{unloaded}}{(\varepsilon_{loaded}+\varepsilon_{unloaded})} \quad (1)$$

Where, σ_{unloaded} and σ_{loaded} are slab bending stresses while $\varepsilon_{\text{unloaded}}$ and $\varepsilon_{\text{loaded}}$ are corresponding strains on unloaded and loaded slabs, respectively.

Deflection based load transfer efficiency LTE (δ) is defined as the ratio of unloaded slab deflection to the loaded slab deflection and can be represented using equation 2.

$$LTE(\delta) = \frac{\delta_{unloaded}}{\delta_{loaded}} \quad (2)$$

Where, δ_{unloaded} and δ_{loaded} are deflections of unloaded and loaded slabs, respectively.

1.2 Modeling of rigid pavements

In rigid pavements, because of concrete's high elastic modulus, the PCC slab supplies most of the structural capacity and tends to transfer the traffic loads to a relatively wider area. Analysis of rigid pavements is a complex and challenging problem due to the presence of longitudinal and transverse joints (discontinuities), a variety of load transfer mechanisms (e.g., dowel bars, aggregate interlocks), and high sensitivity to environmental conditions (e.g., temperature curling, moisture warping). In the early 1920s, rigid pavement response models were developed based on Westergaard's closed-form analytical solutions. The analytical solutions can be used to calculate responses of a single slab under limited loading conditions (Westergaard, 1926a), (Westergaard, 1926b). Finite element models, developed in the early 1960s, can be used to simulate multiple slabs with pavement joints and multi-wheel loads. A number of finite element programs have been developed specifically for rigid pavement analysis (Wei Tu, 2007). Most of these programs use models that are developed based on static analysis assuming that the speed of the vehicle is zero. Research on dynamic response of rigid pavements is limited. Past studies have shown that static loads produce higher stresses than dynamic loads (Chatti et. al., 1994). In

this dissertation, rigid pavement analysis is carried out using two different finite element programs. FEAFAA (Finite Element Analysis – FAA) program is used for pavement analysis under static loading and ABAQUS program is used for dynamic analysis of rigid pavements.

1.3 Airport pavement design

The Federal Aviation Administration (FAA) has developed a mechanistic-empirical design procedure, FAARFIELD, for new and overlay design of flexible and rigid airport pavements. The FAARFIELD (**FAA R**igid and **F**lexible **I**terative **E**lastic **L**ayer **D**esign) program uses layered elastic based and three-dimensional (3D) finite element-based response models to design the pavement thickness (AC 150/5320-6E, 2009). FAARFIELD procedure uses LEAF (layered elastic computational program) mainly for flexible pavement and flexible overlay design and NIKE3D (a three-dimensional finite element analysis program) for design of new rigid pavements and rigid overlays. The NIKE3D version – 3.3.2.FAA.1.0, used in FAARFIELD is a modified FAA version of programs originally developed by the Lawrence Livermore National Laboratory (LLNL) of the US Department of Energy (Kawa et. al., 2007). The FAA has developed a 3D finite element program called FEAFAA (Finite Element Analysis - FAA) for analysis of multiple-slab rigid airport pavements and overlays. FEAFAA can be used for computing stresses, strains and deflections of rigid pavement structures under static aircraft landing gear loads (http://www.airporttech.tc.faa.gov/naptf/, December 2010).

The FAA design standard for pavements is based on a 20-year design life. Airport pavements are designed so that minimum maintenance is required up to 20 years provided that no major variations in traffic forecast are encountered (Garg et. al., 2004). The FAARFIELD program computes the PCC thickness required for an operational life of 20 years for rigid pavements.

The FAARFIELD library has an extensive variety of airplanes with pertinent pavement design characteristics such as taxi weight, annual departures, annual growth rate, tire pressure, tire dimensions, axle spacing, etc. Forecasts of annual departures by airplane type are needed for pavement design. The maximum anticipated take-off weight of the airplane is used for design purposes. The damaging effect of each airplane in the traffic mix is calculated in accordance with Miner's law. This damaging effect is expressed in terms of cumulative damage factor (CDF). The Advisory Circular 150/5320-6E (2009) defines CDF as "the amount of the structural fatigue life of a pavement that has been used up". FAARFIELD iterates on the surface layer thickness until the CDF reaches a value of 1.0 (AC 150/5320-6E, 2009).

$$CDF = \sum_{i=1}^{N} \frac{number\ of\ applied\ load\ repetitions}{number\ of\ allowable\ repetitions\ to\ failure} \quad (3)$$

Where,

N = Number of airplanes in the mix.

Advisory Circular (AC) 150/5320-6E presents the detailed design procedure implemented in the program.

1.4 Problem statement

Since the early 1940's, Westergaard's analysis was adopted for the design of rigid airfield pavements. Based on the full scale traffic tests undertaken at Lockbourne Army Airfield, Ohio, revised rigid pavement design criteria were developed using the Westergaard analysis for edge stresses assuming that properly designed joints would provide a 25 percent load transfer to the adjacent slab. These tests also proved that dynamic loads produce lower stresses in a concrete slab than static loads of equal magnitude (US Army Corps of Engineers, 1946). The mechanistic design procedure (FAARFIELD) developed by the FAA for rigid pavement design continues to

assume 25% stress reduction in the maximum stresses to account for load transfer across the joint. Variations in environmental conditions, loading characteristics, type of joint and pavement material properties can affect load transfer efficiency (Hammons et. al., 1995). Variations in concrete flexural strength and elastic modulus can significantly affect the critical stresses due to aircraft loads. The magnitude of load and aircraft wheel configuration may have an impact on the stresses and LTE at the joint. Also, variations in temperature and moisture content can cause volume changes and slab warping resulting in additional stresses in the slab. When temperature decreases, a joint opening expands, and decreases contact between two slabs and also may decrease the efficiency of the joint. The stress based load transfer efficiency may not remain constant at 0.25 as it depends on external factors mentioned above. Hence, it is necessary to determine the impact of varying pavement material properties, loading intensity, aircraft wheel configuration, and temperature curling on stress based LTE under static loading.

A recently completed study indicates that the dynamic LTE (S) under a moving aircraft gear can be significantly higher than 25% (Wadkar et. al., 2010). Analysis of full scale test data from the National Airport Pavement Test Facility (NAPTF) indicates that LTE (S) under moving loads for Construction Cycle 2 (CC2) test pavement sections is higher than 0.25 (Wadkar et. al., 2010). Yu et. al. studied the dynamic effect of a moving load on LTE by using 3D finite element analysis (Yu et. al., 2010). This study illustrated that LTE (S) under dynamic loading is considerably higher than the static LTE (S). The findings from this study state that the ratio of dynamic LTE (S) to static LTE (S) varies in the range 1 to 2 mainly depending on speed and pavement damping 'C_s'. The dynamic LTE (S) is not sensitive to foundation reaction modulus 'k' and foundation damping 'C_k'. Hence, the dynamic effect is influenced primarily by pavement damping matrix. A higher value of LTE (S) would significantly lower the edge

stresses at the bottom of PCC slab used for thickness design, which, in turn, would lead to significant reduction in slab thicknesses of rigid airport pavements. To obtain accurate dynamic response using 3D finite element analysis, it is necessary to evaluate pavement damping. The effect of dynamic loading on LTE (S) can be studied once the damping parameters for the 3D FEA model are determined. Sensitivity of dynamic LTE (S) to aircraft speed, pavement damping and aircraft wheel configuration is unknown and needs to be determined.

1.5 Hypothesis

Stress based load transfer efficiency is a design variable in the mechanistic design procedure used by the FAA for rigid pavement design. Based on previous research studies and the problem statement, it is hypothesized that:

1) The stress-based load transfer efficiency under dynamic loading is higher than that under static loading.
2) Temperature differentials at the top and bottom of the PCC layer may induce considerable curling stresses in the pavement slabs and may affect the LTE (S) at the joints.
3) LTE (S) is sensitive to PCC and sub-structure material properties, joint stiffness and aircraft wheel configuration.
4) Pavement damping may be the cause of the discrepancies noted between LTE (S) values under static and dynamic conditions.
5) Analysis of rigid pavements under dynamic loading conditions is possible only if the damping parameters are known.

6) The damping in concrete pavements can be determined using measured field data under dynamic loading conditions.
7) The speed of the aircraft can affect the critical tensile strain values at the bottom of PCC layer and also the LTE (S).
8) LTE (S) is sensitive to pavement damping.

1.6 National Airport Pavement Test Facility

The National Airport Pavement Test Facility, located at the Federal Aviation Administration William J. Hughes Technical Center near Atlantic City, New Jersey, USA, is a fully enclosed facility dedicated to full-scale traffic testing of airport pavements under realistic aircraft loads. The data and information collected at the NAPTF is organized by construction cycles. A full construction cycle consists of constructing an instrumented pavement, materials testing, pre-traffic testing, full scale traffic testing, post-traffic testing and pavement removal (http://www.airporttech.tc.faa.gov/naptf/, December 2010). The data pertinent to Construction Cycle 2 (CC2) which consists of rigid pavement test items is used for this analysis. The FAA conducted full-scale traffic tests on CC2 new rigid pavement test items in 2004. The CC2 test sections were named as MRC, MRG and MRS based on their foundation types. M ≡ Medium strength subgrade; R ≡ rigid pavement; C ≡ conventional (aggregate) base; G ≡ pavement on subgrade; S ≡ stabilized (Econocrete) base. The structural properties of the test items are presented in Table 1.

Table 1: Structural Design Data for CC2 Test Items. (Brill, Guo, 2009)

Test Item	**MRC**	**MRG**	**MRS**
PCC Surface	30.5 cm (12 in.) PCC (P-501)	30.5 cm (12 in.) PCC (P-501)	30.5 cm (12 in.) PCC (P-501)
Sub-base 1	25.4 cm (10 in.) aggregate sub-base (P-154)	None	15.2 cm (6 in.) Econocrete base (P-306)
Sub-base 2	None	None	21.9 cm (8.6 in.) Aggregate sub-base (P-154)
Subgrade	Clay (CH) 4 ft. (1.22 m) Medium Strength Subgrade CBR 7	Clay (CH) 4 ft. (1.22 m) Medium Strength Subgrade CBR 7	Clay (CH) 4 ft. (1.22 m) Medium Strength Subgrade CBR 7

Each test item section was 75 ft. long and 60 ft. wide comprising of 20 test slabs of size 15 ft. X 15 ft. The thickness of the slabs was 12 in. and steel dowel bars were used at the joints in both longitudinal and transverse directions. Test items were separated by paved transition areas 25 ft. in length. The dowel bar diameter was 1 in. and the dowel bar spacing was 12 in. The sectional view of CC2 test pavement is shown in Figure 1.

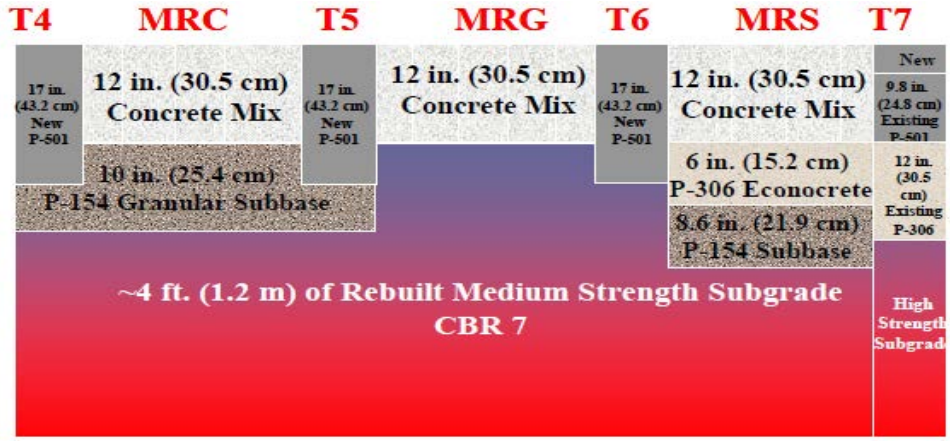

Figure 1: Section view of CC2 test pavement (Ricalde, Daiutolo, 2004)

The facility utilizes the NAPTV (National Airport Pavement Test Vehicle) for loading the test slabs. The NAPTV is programmed for a controlled aircraft wander simulation and can operate with a speed of up to 15 miles per hour (http://www.airporttech.tc.faa.gov/naptf/, December 2010). NAPTV consists of two carriages that can accommodate up to five load modules each comprising two wheels. This allows for configurations of up to 20 wheels with loads up to 75,000 pounds (333.75 kN) per wheel (Brill et. al., 2004). The CC2 test items were planned to be trafficked using the NAPTV wheel configuration shown in Figure 2 using 6-wheel gear configuration on the north side and 4-wheel gear configuration on the south side. However, the test sections were loaded using only 4-wheel gear configuration on both north and south sides with a constant speed at 2.5 miles/hr, tire pressure of 210 psi and a nominal load of 55,000 lbs (244.65 kN) per wheel.

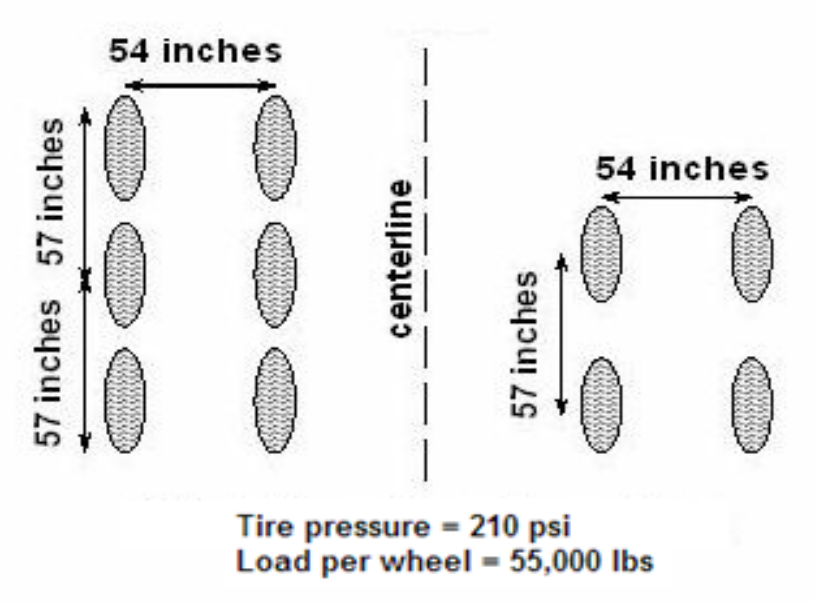

Figure 2: NAPTF wheel configuration (http://www.airporttech.tc.faa.gov/NAPTF/, 2010)

1.7 Objectives of study

The objective of this study is:

1) To determine the LTE (S) of CC2 test sections under dynamic loading conditions using full scale test data from the NAPTF.
2) To study the effect of temperature gradient on critical stresses at the joint.
3) To study the effect of temperature curling on load transfer efficiency of the joint under varying sub-structure conditions.
4) To study the sensitivity of LTE (S) to pavement material properties, joint stiffness and aircraft wheel configuration under static conditions.
5) To develop a 3D FE model for MRC test section and obtain the dynamic responses at the joint under moving aircraft at varying speeds.

6) To study the effect of aircraft speed on tensile strain values at the bottom of PCC at the joint ($\varepsilon_{critical}$).
7) To study the effect of aircraft speed and damping values on dynamic LTE (S) at the joint.

1.8 Significance of Study

The FAA has conducted extensive research to study the impact of pavement material properties and other factors on the operational life of rigid airport pavements. The pavement life is most sensitive to slab thickness, flexural strength of concrete, and aircraft gross weight. The pavement life is slightly sensitive to base thickness and subgrade strength (AC 150/5320-6D, 1995). Rigid airport pavements are constructed in accordance with the requirements contained in Item P-501 which provides guidance on concrete materials, construction methods and quality control of the PCC pavement. Studies have shown that in case of a pavement with P-501 PCC surface, an increase in slab thickness by an inch or increase in flexural strength by 35 psi would increase the pavement's predicted life from 20 to 35 years (Garg et. al., 2004). These predictions are based on theoretical concepts used in failure models and may be different from actual pavement life because of the design assumptions, uncertainties in material properties, climatic conditions and changes in load characteristics.

The FAA has developed FAARFIELD program for the design of airport pavements. For a rigid airfield pavement, FAARFIELD program computes the PCC thickness required for an operational life of 20 years for rigid pavements. The FAA design procedure assumes a value of 0.25 for LTE (S) based upon test sections trafficked from the mid-1940's to the mid-1950's (AC 150/5320-6D, 1995). The LTE at the joint depends on various factors such as type of joint,

construction method, pavement materials, environmental and loading characteristics, etc. Variation in LTE (S) can affect the design edge stresses and also the PCC design thickness. The impact of temperature curling on LTE (S) at the joint is unknown. It is necessary to evaluate the sensitivity of PCC design thickness to varying LTE (S). Previous studies have shown that lower tensile strains values and higher LTE (S) values are obtained under dynamic loading (Yu et. al., 2010). The sensitivity of dynamic LTE (S) to pavement damping, aircraft speed and wheel configuration needs to be determined. The use of a lower LTE (S) design value could result in higher PCC design thickness and excessive pavement structural life.

1.9 Research approach

The approach adopted to achieve the above goal is as follows:

***Task I**: Analysis of full-scale CC2 test data*

The FAA conducted full-scale traffic tests on CC2 new rigid pavement test items in 2004. The heavy weight deflectometer (HWD) data was used to determine the deflection based load transfer efficiency (LTE (δ)). The sensor data from each of the test sections, MRG, MRC and MRS was analyzed. The LTE (S) at the joints under NAPTV loading was determined using the strain gages located on either side of the joint.

***Task II**: Modeling CC2 test pavement using FEAFAA*

The MRG, MRC and MRS sections of the CC2 test pavement were modeled using 3D FE program, FEAFAA. The pavement material properties and thicknesses were obtained from the NAPTF database. The load transfer efficiency for all the three sections under static loading was determined using the FEAFAA model. The sensitivity of LTE (S) to pavement material

properties and joint stiffness was evaluated. The effect of temperature curling on critical edge stresses and LTE (S) was determined. Finally, the sensitivity of LTE (S) to aircraft loading configuration was studied.

***Task III**: Modeling MRC section of CC2 test pavement using ABAQUS*

ABAQUS version 6.10 was used to model MRC rigid pavement section to obtain pavement responses under dynamic loading. The MRC model was calibrated using available HWD test data and dynamic full scale test data from strain gages embedded in MRC slabs. The HWD data and the field data under dynamic loading was obtained from NAPTF database. The concrete damping parameters and the joint stiffness of doweled joints were calibrated using the available HWD data. The ABAQUS MRC model was then validated and verified using the strain gage data. Once the model was verified, the dynamic responses of the test pavement were obtained under varying aircraft speeds. The sensitivity of LTE (S) to pavement damping, aircraft speed, aircraft load and wheel configuration was studied.

1.10 Thesis Outline

This research thesis is divided into seven chapters based on the stated above.

Chapter 1: Introduction

This chapter gives a brief introduction to rigid airport pavements and modeling of rigid airport pavements. The airport pavement design procedure currently used by the FAA is described in this chapter. This chapter presents the problem statement, research hypothesis, objectives, significance of study and the research approach together with a brief background on the National Airport Pavement Test Facility (NAPTF).

Chapter 2: Review of Literature

Because the research includes modeling of rigid pavements, this chapter presents the review of literature on rigid pavement response models including static and dynamic finite element models. Damping phenomena and damping parameters used for modeling are studied in this chapter.

Chapter 3: Analysis of sensor data at NAPTF

The heavy weight deflectometer (HWD) data and the data obtained from concrete strain gage (CSG) sensors embedded in the CC2 test pavement at the NAPTF are analyzed in this chapter.

Chapter 4: Stress-based LTE under static loading

The MRG, MRC and MRS sections of the CC2 test pavement are modeled using FEAFAA to obtain LTE (S) under static loads. The sensitivity of LTE (S) to concrete and base properties, temperature gradient, joint stiffness and aircraft configuration is studied.

Chapter 5: Stress-based LTE under moving aircraft

The MRC section of the CC2 test pavement is modeled using ABAQUS to obtain dynamic pavement responses under moving aircraft loads. The effect of aircraft speed and pavement damping on critical tensile strains and LTE (S) at the joint is analyzed in this chapter.

Chapter 6: Summary of findings, conclusions and recommendations

The final chapter of this thesis highlights the most significant outcomes and contributions of this research. Finally, the recommendations for further studies based on research findings are outlined.

1.11 Summary

This chapter gave a brief overview of the problem statement and objectives of this study. Load transfer among slabs is an important factor in rigid pavement design and construction. The impact of pavement characteristics, loading intensity, aircraft wheel configurations and speed on load transfer efficiency is studied in this research project. The CC2 test pavement sections were modeled using various 3D finite element programs. The full scale test data from the NAPTF was used for this analysis. The research approach adopted for this study is outlined in this chapter.

CHAPTER 2

Review of Literature

2.1 Response models for rigid pavements

In the past, rigid pavements have been designed using the Westergaard theory. In the 1920s, Westergaard developed analytical solutions for analyzing concrete pavements using the classical thin-plate theory. Westergaard's analytical solutions had following limitations:

a) The concrete slab is assumed to be thin, homogenous and elastic
b) The concrete slab is assumed to be resting on a Winkler foundation which is characterized by a single variable – modulus of subgrade reaction (k).
c) Stresses and deflections can be only calculated for center, edge and corner loadings
d) Shear and frictional forces acting on concrete slab surfaces are ignored
e) Discontinuities in concrete slab due to cracks / joints are not considered
f) The method was developed for single wheel load only

Since the original work done by Westergaard, researchers have improved the methods used for stress calculation. Pickett and Ray (1951) developed influence charts that allow the Westergaard equations to be applied to multiple wheel loadings. Salsilli et al. (1993) applied the Newton-Raphson iteration procedure to convert multiple wheel loadings to an equivalent single loaded area that would produce the same bending stress and used this transformed loading in Westergaard's equations.

2.2 Finite element models for rigid pavement analysis

Analytical closed-form solutions are desirable in routine pavement analysis and design. However, the assumptions made to develop those solutions place too many limitations on the application. Due to these limitations the use of finite element method for rigid pavement analysis gained popularity since the early 1970s. A two dimensional (2-D) linear elastic finite element model was developed by Wang (1972) to study the rigid pavement responses under wheel loads. Another 2-D finite element model was developed by Huang in 1974. This model considered the effect of load transfer across adjacent slabs. With the advent of these 2-D elastic finite element models, various general 2-D finite element programs such as ILLI-SLAB (1978), WESLAYER (1981), JSLAB (1984), KENSLAB (1985), etc., were developed. A 3-D, nonlinear, static, finite element model was developed by Channakeshava et al. (1993) to study the pavement response with doweled joints. Another 3-D, nonlinear finite element model was developed by Zaghloul et al. (1994) using ABAQUS program. A list of some of the commonly used programs for pavement analysis with model parameters and load type used is given in Table 2.

Table 2: Programs developed for pavement analysis (Wei Tu, 2007)

FEM Program	**Dimensions**	**Slab Model**	**Subgrade Model**	**Material Model**	**Load**
ILLI-SLAB	2-D	Medium-thick Plate Element	Winkler	Linear Elastic	Static
JSLAB	2-D	Medium-thick Plate Element	Winkler	Linear Elastic	Static
WESLAYER	2-D	Medium-thick Plate Element	Elastic Solid/ Layers	Linear Elastic	Static
KENSLAB	2-D	Medium-thick Plate Element	Winkler/ Elastic Solid/ Elastic Layers	Linear Elastic	Static
RISC	2-D	Medium-thick Plate Element	Elastic Solid/ Elastic Layers	Linear Elastic	Static
FEACONS	2-D	Medium-thick Plate Element	Winkler	Linear Elastic	Static
DYNA-SLAB	2-D	Medium-thick Plate Element	Damped Winkler/ Layered Solid	Linear Elastic	Dynamic
EVERFE	3-D	Quadratic Hexahedral Elements	Winkler	Linear Elastic	Static

Most of the finite element models are based on static aircraft loading although realistic aircraft loading is dynamic in nature. Experimental tests on concrete pavements conducted by The American Association of State Highway and Transportation Officials (AASHTO) showed that an increase in vehicle speed from 3.2 to 95.6 km/h (2 to 60 mph) decreased the pavement responses by about 29 per cent (AASHTO, 1962). To study the effects of dynamic loading on rigid pavements, Chatti et al. (1994) developed a linear dynamic finite element program, called DYNA-SLAB.

Some researchers believe that dynamic effects of vehicles can amplify the propagation of existing cracks resulting in further damage to the pavement. It has been found that pavement surface unevenness, structural variability and the dynamic wheel loads cause wear to the pavement (Gillespie et. al., 1993). Pavement fatigue can be attributed to the combined effect of large traffic volumes carrying heavy loads under high speeds. Even though static loads produce higher stresses than dynamic loads, dynamic analysis cannot be neglected. The dynamic pavement responses of a pavement slab can be obtained using direct integration method.

$$[M]\{\ddot{w}\} + [C]\{\dot{w}\} + [K]\{w\} = \{F\} \quad (4)$$

Where:

$[M]$ = mass matrix of pavement structure;

$[K]$ = stiffness matrix of foundation;

$\{F\}$ = column vector of external force;

$[C]$ = damping matrix of pavement structure; and, $[C] = [C_s] + [C_k]$ (5)

$[C_s]$ = pavement damping matrix;

$[C_k]$ = foundation damping matrix.

Table 3 provides the summary of literature review on rigid pavement analysis using finite element models. Table 4 gives a summary of literature review on rigid pavement analysis using ABAQUS program. The findings from the literature review helped the author understand finite element modeling of rigid airfield pavements under static and dynamic loading conditions and its effect on load transfer efficiency.

Table 3: Summary of literature review on analysis of rigid pavements

Sl. No.	Title	Author	Type of Analysis	Software Used	Model Type / Elements Used	Key Findings
1	Finite Element Analysis of Concrete slabs and its implications for Rigid Pavement Design (1973)	Y. H. Huang, S. T. Wang	2D Finite Element Analysis	Unknown	The model consists of thin plates on Winkler foundation	• Stresses at the joint are less critical due to load transfer • The edge stresses should be used for the design of the pavements instead of joint stresses
2	Dynamic Finite-Element Analysis of Jointed Concrete Pavements (1994)	Karim Chatti	2D Finite Element Analysis	DYNA-SLAB	• The concrete slab is modeled by rectangular medium-thick plate elements • The foundation support is represented by a damped Winkler foundation model • Load transfer across joints is modeled either by a vertical spring element to represent aggregate interlock, or by a bar element to represent dowel bars	• Dynamic analysis is generally not needed for the design of rigid pavements as it usually leads to decreased pavement response • A quasi-static analysis gives conservative results provided that the wheel loads used in the analysis have been adjusted for the effects of vehicle velocity, truck suspension characteristics, and pavement roughness.

3	Component Dowel-Bar Model for Load-Transfer Systems in PCC Pavements (1995)	E. H. Guo, James A Sherwood, Mark B. Snyder	A component dowel bar model is developed to simulate doweled joint in PCC	-	The model consists of 2 bending beams of finite length connected by a shear bending beam	The model can be integrated into Finite Element program to obtain distributions of bending moment, bearing stress and shear force at each dowel
4	Back Estimation of slab curling and joint stiffness (2001)	E. H. Guo	2D Finite Element Analysis	JSLAB	-	• The sum of the HWD deflections (SD) on the two sides of the dummy joints increases proportionally to the slab curling but are insensitive to LTE (d). • SD can be used to back estimate the slab curling defined by equivalent temperature gradient "g". • The joint stiffness 'K_d' may also be back-calculated.
5	Field and analytical investigations of dowel performance in transverse joint	Fouad Fanous; Dominique Shannon	3D Finite Element Analysis	ANSYS (2007)	• The Macro capabilities available in ANSYS (2007) software are used to model a PCC pavement structure	• Dowels with larger diameter with 12 in. spacing resulted in the highest LTE. • The effect of the modulus of dowel support on the LTE is insignificant.

	of concrete pavement (2008)				• Brick elements were used to idealize PCC pavement and 3D beam elements were used to idealize dowel bars	
6	Joint load transfer efficiency of rigid pavement considering dynamic effects under a single moving load (2010)	Xinhua YU, Yumin ZHOU	3D Finite Element Analysis	ANSYS (2007)	• Kelvin foundation is used to simulate the subgrade • Aggregate interlock and dowel bar embedment is reflected by a set of joint shearing springs	• LTE(S) increases with the speed of the moving wheel. • LTE(S) is directly proportional to the pavement damping Cs. • The ratio dynamic LTE(S) to static LTE(S) varies in the range 1 to 2 mainly depending on speed ‘v’ and damping ‘C_s’. • The dynamic LTE(S) is not sensitive to foundation reaction modulus ‘k’ and foundation damping ‘C_k’.

Table 4: Summary of literature review on pavement analysis using ABAQUS models

Sl. No	Title	Author	Element used	Model Type	Interface between layers	Loading	Verified with	Key Findings
1	Investigation of Load Equivalent Factors	Zaghloul et al. (1994)	3D Brick	• Bi-linearly elastic-plastic solid concrete model • Elastic-Plastic Druker-Prager base model • Cam-Clay subgrade model	DNA	Static	Westergaard's analytical solution	• The predicted deflections for static loading were in close agreement with the analytical solutions.
2	Investigation of various factors affecting rigid pavement support	Darter et al. (1995)	2D plate; 3D brick	• Linearly elastic concrete model • Linearly elastic base model • Winkler Foundation	Membrane Element Coupled with a Special Interface Element	Static	Westergaard's analytical solution, ILLISLAB, AASHTO road test	• Good agreement was found for the cases when 2-D plate elements were applicable, i.e., thin slab with fairly large loading area. • The predicted pavement responses from the model were also compared with full-scale field test data from the AASHO Road 33

3	Response of Rigid Pavement to the thermal loading	Masad et al. (1996)	8 node brick elements	• Linearly elastic concrete model • Linearly elastic base model • Linearly elastic foundation model	Friction and Loss of Contact between Slab and Foundation	Static	ILLISLAB-JSLAB	• The model results indicated that maximum curling stresses, for the entire range of the linear temperature gradient analyses, were about 28 percent of the concrete modulus of rupture. • They reported that nonlinear temperature gradient caused higher tensile stresses than the linear one. • Coefficient of friction at slab/base interface had minimal effect on curling stress.
4	Response of a single rigid pavement slab to the heavy multiple-wheel loading	Kim et al. (1997)	linear hexa-hedral elements	• Linearly elastic concrete model • Non-Linear Drucker-Prager Elasto-Plastic base model • Linearly elastic foundation model	Bonded and Un-bonded Conditions	Static	DNA	• Maximum deflections were generally proportional to the total load regardless of wheel configuration. However, the maximum stresses in the slab were governed by the curvature of the slab, which greatly depends on the wheel spacing. • The smaller the wheel spacing, the higher the stresses due to the

								high interaction between the wheels.
5	Modeling of the Stresses and Strains Distribution in an RCC Pavement	Zdiri et. Al. (1999)	Hexahedrons with 8 nodes	• Linearly elastic concrete model • Linearly elastic base model • Solid foundation model	Partial Contact Between Layers	Static	2D models	• The solid foundation is more realistic than the liquid foundation, because the deflection in any nodal point depends not only on the force in this node but also of the forces in all the other nodes. • The use of assumptions of the partial contact between foundation layers is more realistic than perfect contact. • The results obtained from 3D modeling using ABAQUS gives slightly lower stresses and higher deflections than that obtained from closed form solutions

6	The effects of joint opening on LTE	Ali Mansour Khaki; Ehsan Azadraves	C3D8R-Bricks	• concrete damage plasticity model • Linear elastic base model • Winkler foundation model	Surface to Surface Hard Contact	Static	DNA	• When the concrete slab contracts & joint opens, aggregate interlock is lost & LTE decreases significantly. • Using base layer under slabs in designing concrete pavements, increases load transfer efficiently. • The decrease of load transfer efficiency due to joint opening is a big problem for aged concrete pavements & pavements with loose dowels

2.3 Damping

The phenomenon of dissipation of energy in the system through various mechanisms is called damping. In damping, the amplitude of free vibration steadily diminishes (Dynamics of Structures, 3rd edition, 2007). Damping in complex structures can be represented by a linear viscous damper or dashpot as it is practically not possible to mathematically identify all the energy dissipating mechanisms in such structures. Thus, damping in actual structures is usually represented by equivalent viscous damping. The equation of motion governing the displacement $u(t)$ of a linear elastic system subjected to an external dynamic force $p(t)$ is given by (Dynamics of Structures, 3rd edition, 2007):

$$m\ddot{u} + c\dot{u} + ku = p(t) \tag{6}$$

Where,

m = mass of the system

c = damping coefficient

k = stiffness of the system

If the system is considered as a combination of three pure components: stiffness component, mass component and damping component then the external force $p(t)$ can be distributed as:

$$p(t) = f_S + f_I + f_D \tag{7}$$

And, $$f_S = ku; \quad f_I = m\ddot{u}; \quad f_D = c\dot{u}$$

Setting $p(t) = 0$ in equation 7 gives the differential equation governing free vibration of the system with damping.

$$m\ddot{u} + c\dot{u} + ku = 0 \tag{8}$$

Dividing by m gives,

$$\ddot{u} + 2\zeta\omega_n\dot{u} + \omega_n^2 u = 0$$

Where,

$\omega_n = \sqrt{k/m}$ = natural circular frequency

$\zeta = \frac{c}{2m\omega_n} = \frac{c}{c_{cr}}$ = damping ratio

$c_{cr} = 2m\omega_n = 2\sqrt{km} = \frac{2k}{\omega_n}$ = critical damping coefficient

If $c < c_{cr}\ or\ \zeta < 1$, the amplitude of oscillation diminishes gradually and the system returns to equilibrium position. For cases when $c = c_{cr}\ or\ \zeta = 1$ and $c > c_{cr}\ or\ \zeta > 1$, the system does not oscillate and arrives back to its equilibrium position quickly. The damping coefficient c_{cr}, also known as the critical damping coefficient is the smallest value of *c* that prevents oscillations in the system (Dynamics of Structures, third edition, 2007).

The total energy in a freely vibrating system is made up of two parts, kinetic energy E_K and potential energy E_S. Thus the total energy is

$$E_K(t) + E_S(t) = \frac{1}{2}k[u(0)]^2 + \frac{1}{2}m[\dot{u}(0)]^2 \quad (9)$$

In viscously damped systems, the total energy decreases with time because of energy dissipated through damping. The dissipated energy over the time duration 0 to t_1 is given by:

$$E_D = \int f_D du = \int_0^{t_1} (c\dot{u})udt = \int_0^{t_1} c\ddot{u}dt \quad (10)$$

As time t_1 goes to ∞, the dissipated energy given by equation 10 tends to equal the input energy given by equation 9.

Experiments on structural metals have indicated that energy is dissipated internally due to cyclic straining of the material. This type of damping is referred as rate independent linear damping as the energy dissipated is independent of cyclic frequency. Other terms used for this mechanism are structural damping / hysteretic damping. Rate independent damping is associated with static hysteresis due to plastic strain, localized plastic deformation, crystal plasticity, and plastic flow

in a range of stresses within the apparent elastic limit (Dynamics of Structures, 3rd edition, 2007).

2.3.1 Rayleigh Damping

Rayleigh damping is a simplified form of viscous damping. Rayleigh damping is proportional to the stiffness and mass of the structure and can be defined using equation 11.

$$[\mathrm{C}] = \alpha[\mathrm{M}] + \beta[\mathrm{K}] \tag{11}$$

Where,

[C] = damping matrix of the physical system (lbf-s/ft^3)

[M] = mass matrix of the physical (lb)

[K] = stiffness matrix of the system (pci)

α = mass proportional damping coefficient (1/s)

β = stiffness proportional damping coefficient (s)

This type of damping is used in most mathematical models since it eliminates the need to form a damping matrix based on physical properties of the structure (Dynamics of Structures, 3rd edition, 2007).

For a given mode 'i' the damping ratio 'ζ' can be expressed in terms of the damping factors α and β as:

$$\zeta_i = \frac{\alpha}{2\omega_i} + \frac{\beta\omega_i}{2} \tag{12}$$

Where, ω_i is the natural frequency at this mode.

The damping forces caused by the absolute velocities of the model are represented by the mass proportional damping coefficient 'α'. The model simulates the idea of moving through viscous "ether" (a permeating, still fluid) so that any motion of any point in the model causes damping

(ABAQUS user manual, 2010). The mass proportional damping coefficient 'α' introduces damping in the system proportional to the mass matrix for an element.

The 'β' factor introduces damping proportional to the strain rate, which can be thought of as damping associated with the material itself. 'β' defines damping proportional to the elastic material stiffness (ABAQUS user manual, 2010).

Equation 12 implies that the mass proportional Rayleigh damping, α, damps the lower frequencies and the stiffness proportional Rayleigh damping, β, damps the higher frequencies.

2.4 Summary

A detailed literature review about rigid pavement response models was conducted. Finite element programs commonly used for rigid pavement analysis were studied. A majority of finite element programs use linear elastic model and static loading conditions. Some authors believe that dynamic effects of vehicles can amplify the propagation of cracks and hence pavement response under dynamic loading needs to be studied. Rayleigh damping is generally used in mode-based linear dynamic mathematical models for the simulation of the dynamic response of a structure. Rayleigh damping is proportional to the stiffness and mass of the structure. The CC2 test sections are modeled using ABAQUS to study the dynamic responses under NAPTV loading. Pavement damping in ABAQUS is simulated using Rayleigh damping.

Chapter 3

Analysis of sensor data at NAPTF

3.1 Full scale testing at NAPTF

As mentioned in chapter 1, the test items of CC2 consisted of three rigid pavements constructed on granular conventional base (MRC), on grade (MRG) and on stabilized Econocrete base (MRS). The test sections are constructed over a medium strength subgrade of CBR = 7. Each test item section was 75 ft. long and 60 ft. wide, comprised of 20 slabs of size 15 ft. x 15 ft.

The slabs are numbered sequentially from west to east starting from the north-west corner of MRC and ending with the south-east corner of MRS. Thus the MRC section consists of slabs numbered from 1 to 20, the MRG section consists of slabs numbered 21 to 40 and the MRS section consists of slabs numbered from 41 to 60. Figure 3 shows the numbering of slabs for all three test items in MRC/MRG/MRS format.

	1/21/41	2/22/42	3/23/43	4/24/44	5/25/45
North Carriage	6/26/46	7/27/47	8/28/48	9/29/49	10/30/50
	11/31/51	12/32/52	13/33/53	14/34/54	15/35/55
South Carriage	16/36/56	17/37/57	18/38/58	19/39/59	20/40/60

Figure 3: Typical plan view of CC2 test items with slab numbers (Wadkar, 2010)

The PCC slabs were 12 in. in thickness. The interior slabs are connected with steel dowels on all four sides while the outer slabs are connected with dowels on three sides, leaving only the free outer edges non-doweled. Curling of the slabs was measured to be 20 mils or less (Daiutolo, 2008).

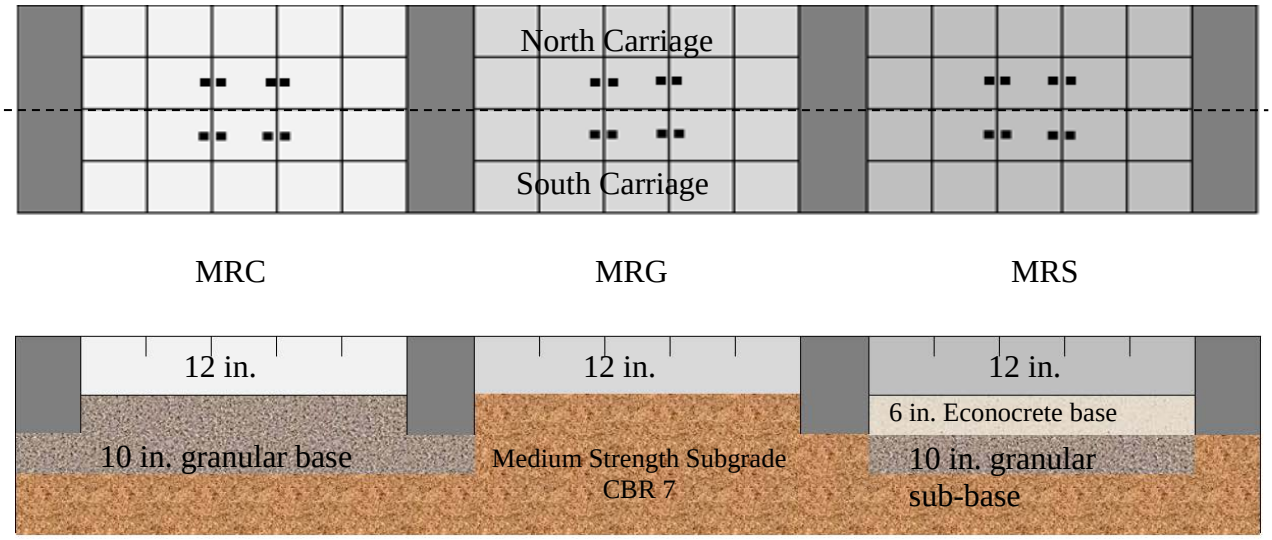

Figure 4: Plan and sectional view of CC2 test items (Wadkar, 2010)

The CC2 test items are loaded using the National Airport Pavement Test Vehicle (NAPTV) which is programmed for controlled aircraft wander simulation. The wander pattern used for CC2 trafficking had 66 discrete positions approximating a normal traffic distribution. Both the north and south test sections were loaded with a dual tandem carriage configuration (Brill and Guo 2009).

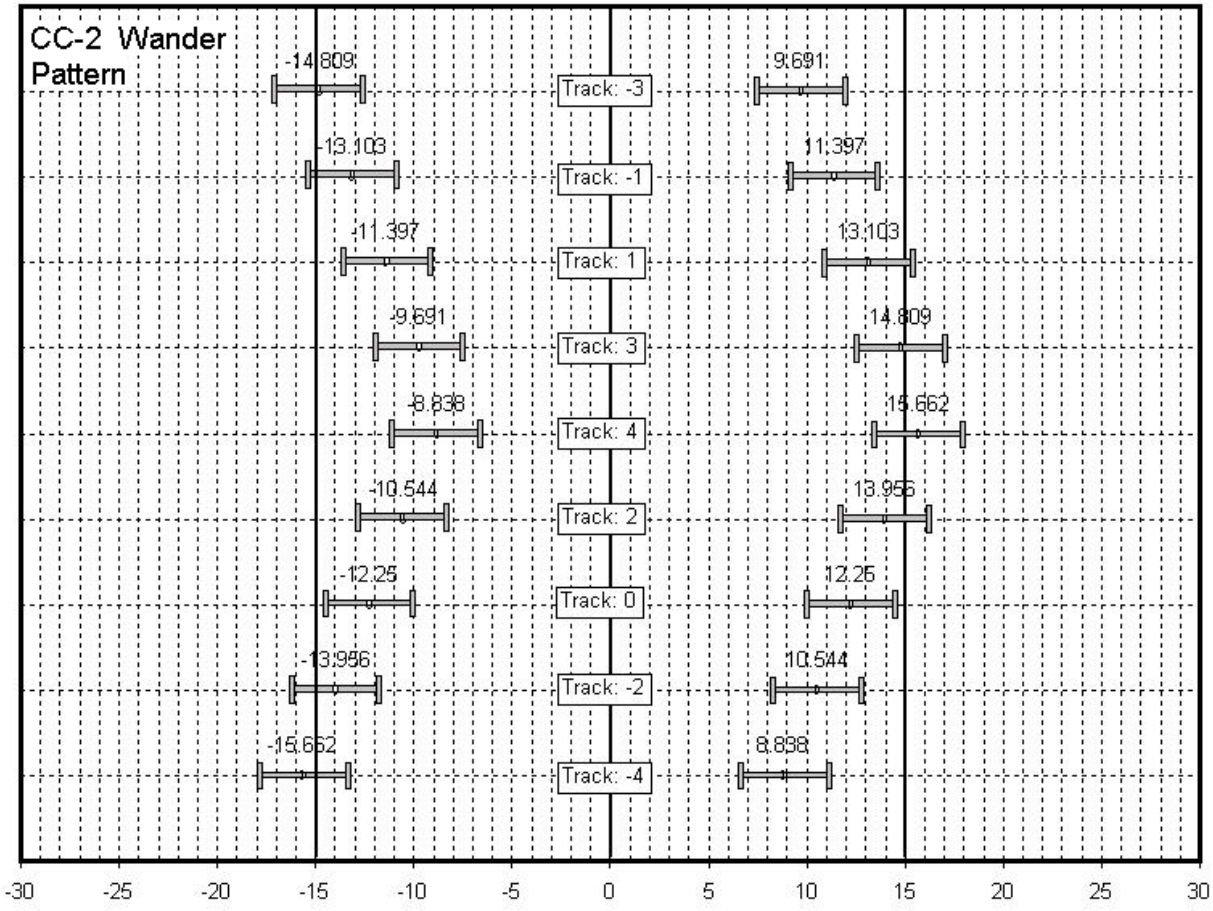

Figure 5: CC2 wander pattern (http://www.airporttech.tc.faa.gov/NAPTF/, 2010)

Traffic on test item MRC began on April 27 and ended on June 24, 2004. Traffic on test items MRG and MRS began on July 6 and ended on December 10, 2004. The nominal load for all tests was 55,000 lbs per wheel at 210 psi tire pressure. A summary of the traffic applied to each test item is presented in Table 5. Trafficking of the NAPTV from West to East or East to West is equivalent to one 'pass'. The dynamic response for the passes in which one set of wheels of NAPTV pass directly over the embedded strain sensors are used for this analysis.

Table 5: Traffic Summary for CC2 Test Items. (Brill et. al., 2005)

Test Item	**Gear Type**	**Passes completed**			
		Apr-Jun 2004	**Jul-Sep 2004**	**Oct-Dec 2004**	**Total**
MRC – North	4-wheel	12675	0	0	12675
MRC – South	4-wheel	5405	0	0	5405
MRG – North	6-wheel	0	21186	9834	31020
MRG – South	4-wheel	0	21186	9834	31020
MRS – North	6-wheel	0	20262	0	20262
MRS – South	4-wheel	0	21162	9834	30996

The CC2 test pavement was installed with concrete strain gages at various locations, including locations on each side of joints, to measure the strains. Figure 6 shows the location co-ordinates for slabs and sensors embedded in MRC section of CC2 test pavement. The sensors are located near the top of PCC (z location = 0.125 ft. from the surface) and near the bottom of PCC (z location = 0.875 ft. from the surface).

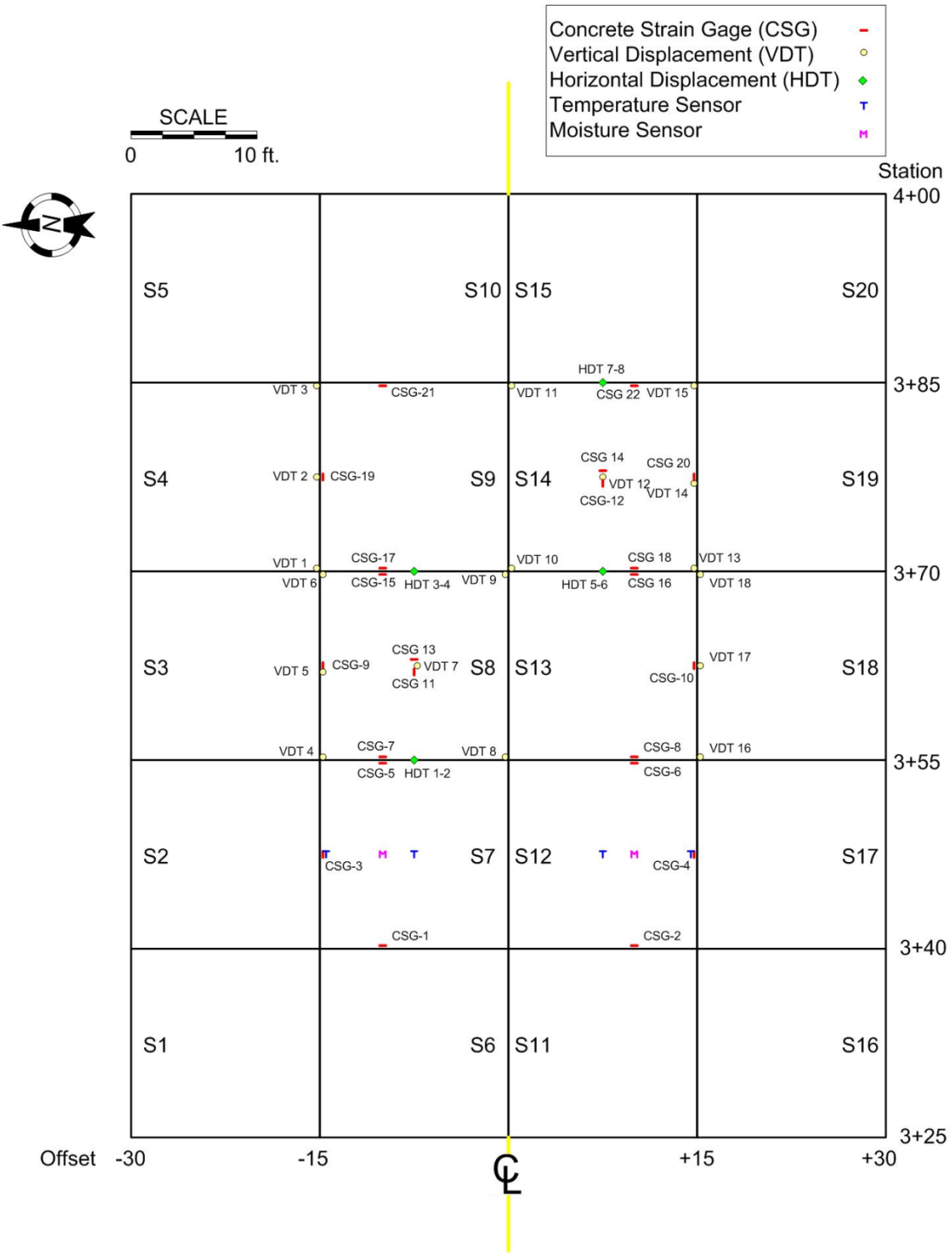

Figure 6: Slab co-ordinates and location of sensors for MRC section

(http://www.airporttech.tc.faa.gov/NAPTF/, 2010)

The raw data from the embedded concrete strain gages (CSG) was obtained from the NAPTF database. To calculate the stress based load transfer efficiency, the raw data required some processing and synchronization (Wadkar, 2010). The synchronization process was based on the known time lag between the first and second peaks of the strain profiles as both the axles pass over the sensors located on either side of the joint with constant speed. Using the speed of the test vehicle, distance between the front and rear axles, and distance between the sensors, the time lag was expected to be 0.136 seconds. The strain profiles are adjusted to match the time lags between the first and second peaks before calculating LTE (S). The detailed process of synchronization is presented in Wadkar et. al. (2010).

Strain sensors CSG-5 and CSG-7 are embedded in slabs S7 and S8 respectively on either side of the joint as shown in figure 7.

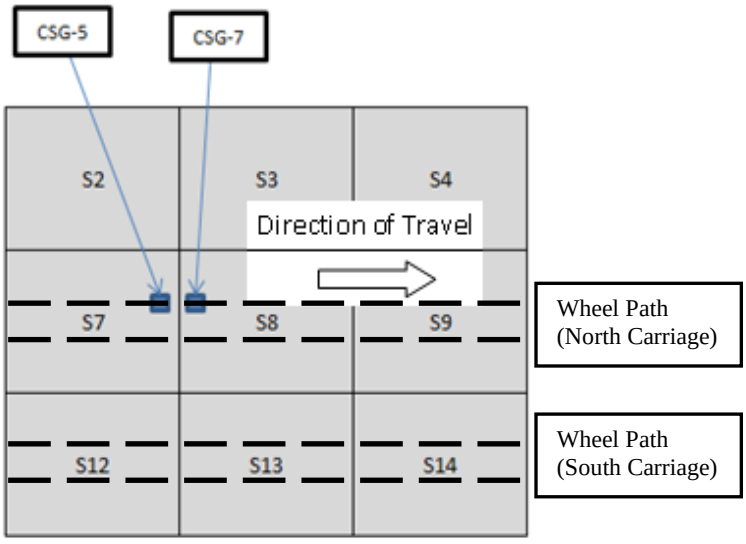

Figure 7: Location of concrete strain gages (CSG) in MRC section

3.2 LTE (S) from strain gage analysis

Peak strains recorded by the pair of gages located on either side of the joint as the test vehicle traversed the joint were used to calculate the stress-based load transfer efficiency. Only those passes in which the wheels of the test vehicles passed directly over the strain gages were used for calculation of LTE (S). In the CC2 database, those passes are termed as the Track 0 events. Pairs of strain gages on either side of the transverse joint are analyzed for each of the three test sections for Track 0 events. Table 6 shows a list of strain gages analyzed for the MRC, MRG and MRS test sections with their locations along X, Y and Z direction.

Table 6: Traffic Summary for CC2 Test Items.

Sensor name	**Sensor type**	**Test Item**	**Location X (ft)**	**Location Y (ft)**	**Location Z (ft)**	**Comment**
CSG-5	Concrete Strain	MRC	354.75	-10	0.875	Transverse Joint
CSG-7	Concrete Strain	MRC	355.25	-10	0.875	Transverse Joint
CSG-28	Concrete Strain	MRG	454.75	10	0.875	Transverse Joint
CSG-30	Concrete Strain	MRG	455.25	10	0.875	Transverse Joint
CSG-52B	Concrete Strain	MRS	555.25	10	0.875	Transverse Joint
CSG-54C	Concrete Strain	MRS	554.75	10	0.875	Transverse Joint

The LTE can be calculated for four distinct cases using strain profiles for any event from each of the above listed strain gages. A ‘Go’ event is the event when the vehicle traverses from West to

East and a ‘Return’ event is the event when the vehicle traverses from East to West. The four cases of LTE (S) are when the carriage is at Position 1 in the ‘Go’ direction, Position 4 in the ‘Go’ direction, Position 4 in the ‘Return’ direction and Position 1 in the ‘Return’ direction. Positions 1 through 4 are defined for the purpose of this study and are represented in figure 8 (Wadkar, 2010). For a vehicle traveling West to East (‘Go’ pass), Position 1 is when all wheels are on the loaded slab just before the transverse joint. Position 4 is when all wheels are on the other side of the transverse joint and are on the adjacent slab which is now the loaded slab. For a ‘Return’ pass (East to West), the positions are switched.

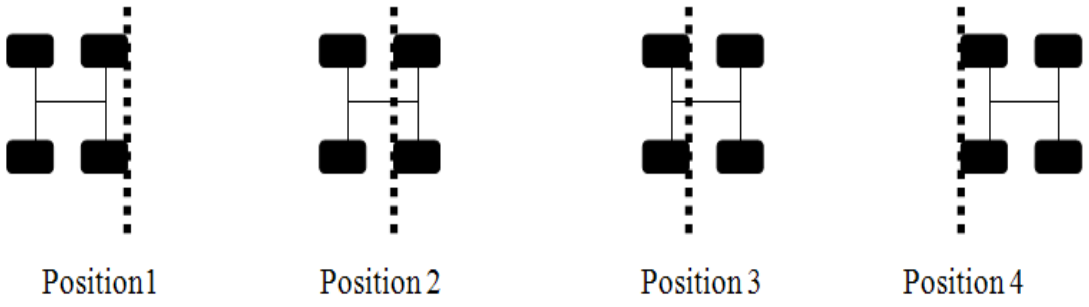

Figure 8: Test vehicle positions in reference to the transverse joint (Wadkar, 2010)

The strain profiles for CSG-5 and CSG-7 for a typical ‘Go’ pass are shown in figure 9. The LTE (S) for position 1 is calculated using the peak strain value for CSG-5 and the corresponding strain value for CSG-7 at that instant.

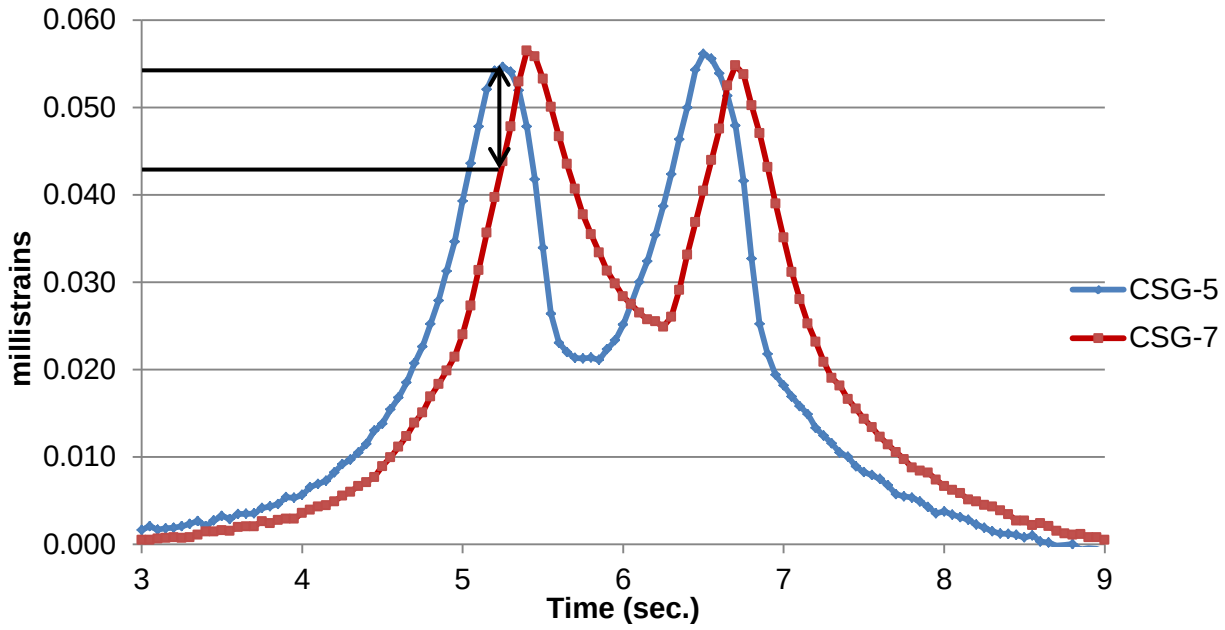

Figure 9: Loaded and unloaded strain profiles for moving aircraft

From the above graph dynamic LTE (S) for position 1 is calculated as follows:

$$LTE(S) = \frac{\varepsilon_U}{(\varepsilon_U + \varepsilon_L)} = \frac{\varepsilon_{CSG-7}}{\varepsilon_{CSG-7} + \varepsilon_{CSG-5}} \quad (13)$$

$$LTE(S) = \frac{0.044}{0.044 + 0.055} = 0.445$$

The LTE (S) for MRC, MRG and MRS was calculated for the first 20 passes (both 'Go' and 'Return' events) for position 1 and position 4 using the method mentioned above.

Table 7 gives the calculated LTE (S) for the first 20 Track 0 passes ('Go' and 'Return' events) for position 1 and position 4 for CC2 MRC section. Table 8 presents the calculated LTE (S) for the first 20 'Track 0 passes' for position 1 and position 4 for CC2 MRG section. Table 9 presents the calculated LTE (S) for the first 20 'Track 0 passes' for position 1 and position 4 for MRS test section.

Table 7: LTE (S) for MRC section

MRC	LTE (S) for Position 1				LTE (S) for Position 4			
	Go (W to E)		Return (E to W)		Go (W to E)		Return (E to W)	
Pass #	Event	LTE(S)	Event	LTE(S)	Event	LTE(S)	Event	LTE(S)
1	1394	0.45	1395	0.44	1394	0.47	1395	0.5
2	1404	0.46	1405	0.45	1404	0.45	1405	0.5
3	1412	0.47	1413	0.44	1412	0.49	1413	0.51
4	1420	0.45	1421	0.45	1420	0.46	1421	0.51
5	1426	0.46	1427	0.46	1426	0.49	1427	0.51
6	1442	0.47	1443	0.46	1442	0.49	1443	0.5
7	1450	0.47	1451	0.49	1450	0.5	1451	0.5
8	1458	0.44	1459	0.44	1458	0.46	1459	0.49
9	1464	0.44	1465	0.47	1464	0.46	1465	0.48
10	1470	0.44	1471	0.47	1470	0.46	1471	0.45
11	1480	0.42	1481	0.47	1480	0.46	1481	0.45
12	1488	0.42	1489	0.47	1488	0.45	1489	0.45
13	1496	0.4	1497	0.44	1496	0.48	1497	0.45
14	6871	0.5	6872	0.38	6871	0.36	6872	0.47
15	6881	0.51	6882	0.43	6881	0.43	6882	0.51
16	6890	0.4	7024	0.45	6890	0.47	7024	0.47
17	7093	0.47	7094	0.4	7093	0.32	7094	0.45
18	7099	0.47	7109	0.45	7099	0.42	7109	0.43
19	7110	0.41	7117	0.4	7110	0.47	7117	0.48
20	7118	0.4	7125	0.45	7118	0.45	7125	0.42
	AVG	**0.45**	**AVG**	**0.45**	**AVG**	**0.45**	**AVG**	**0.48**

Table 8: LTE (S) for MRG section

MRG	LTE (S) for Position 1				LTE (S) for Position 4			
	Go (W to E)		Return (E to W)		Go (W to E)		Return (E to W)	
Pass #	Event	LTE(S)	Event	LTE(S)	Event	LTE(S)	Event	LTE(S)
1	14091	0.44	14092	0.46	14091	0.54	14092	0.48
2	14109	0.43	14110	0.48	14109	0.55	14110	0.5
3	14133	0.42	14134	0.44	14133	0.52	14134	0.48
4	14139	0.42	14140	0.46	14139	0.54	14140	0.48
5	14151	0.43	14152	0.46	14151	0.53	14152	0.48
6	14157	0.42	14158	0.46	14157	0.53	14158	0.47
7	14175	0.43	14176	0.46	14175	0.52	14176	0.47
8	14199	0.42	14200	0.46	14199	0.49	14200	0.48
9	14205	0.43	14206	0.47	14205	0.52	14206	0.46
10	14217	0.42	14218	0.47	14217	0.55	14218	0.46
11	14223	0.41	14224	0.46	14223	0.5	14224	0.47
12	14241	0.41	14242	0.47	14241	0.49	14242	0.48
13	14265	0.42	14266	0.45	14265	0.53	14266	0.47
14	14271	0.4	14272	0.46	14271	0.51	14272	0.47
15	14283	0.42	14284	0.46	14283	0.53	14284	0.48
16	14289	0.41	14290	0.48	14289	0.52	14290	0.48
17	14307	0.41	14308	0.44	14307	0.53	14308	0.48
18	14331	0.41	14332	0.45	14331	0.54	14332	0.49
19	14337	0.41	14338	0.47	14337	0.53	14338	0.49
20	14349	0.41	14350	0.43	14349	0.56	14350	0.46
	AVG	**0.42**	**AVG**	**0.46**	**AVG**	**0.53**	**AVG**	**0.48**

Table 9: LTE (S) for MRS section

MRS	LTE (S) for Position 1				LTE (S) for Position 4			
	Go (W to E)		Return (E to W)		Go (W to E)		Return (E to W)	
Pass #	Event	LTE(S)	Event	LTE(S)	Event	LTE(S)	Event	LTE(S)
1	14091	0.49	14092	0.44	14091	0.45	14092	0.49
2	14109	0.49	14110	0.44	14109	0.48	14110	0.5
3	14133	0.45	14134	0.47	14133	0.49	14134	0.51
4	14139	0.49	14140	0.46	14139	0.47	14140	0.52
5	14151	0.45	14152	0.42	14151	0.42	14152	0.5
6	14157	0.46	14158	0.46	14157	0.48	14158	0.52
7	14175	0.45	14176	0.44	14175	0.45	14176	0.52
8	14199	0.43	14200	0.41	14199	0.41	14200	0.48
9	14205	0.46	14206	0.43	14205	0.51	14206	0.51
10	14217	0.48	14218	0.43	14217	0.5	14218	0.53
11	14223	0.46	14224	0.41	14223	0.46	14224	0.52
12	14241	0.45	14242	0.43	14241	0.49	14242	0.5
13	14265	0.48	14266	0.45	14265	0.46	14266	0.54
14	14271	0.46	14272	0.42	14271	0.5	14272	0.52
15	14283	0.46	14284	0.41	14283	0.51	14284	0.55
16	14289	0.46	14290	0.42	14289	0.5	14290	0.52
17	14307	0.48	14308	0.41	14307	0.47	14308	0.53
18	14331	0.42	14332	0.4	14331	0.41	14332	0.56
19	14337	0.44	14338	0.45	14337	0.49	14338	0.53
20	14349	0.47	14350	0.38	14349	0.48	14350	0.54
	AVG	**0.46**	**AVG**	**0.43**	**AVG**	**0.47**	**AVG**	**0.52**

From the analysis conducted above, it is observed that the LTE (S) under moving loads for CC2 test item joints was found to be within a range of 40% to 56%. Table 10 provides a summary of average LTE (S) values for position 1 and position 4 for the first 20 Track 0 passes for CC2 test sections.

Table 10: Average LTE (S) values for CC2

Section	Position 1		Position 4	
	Go	Return	Go	Return
MRC	0.45	0.45	0.45	0.48
MRG	0.42	0.46	0.53	0.48
MRS	0.46	0.43	0.47	0.52

Variability in the LTE (S) values may be due to the variability in the recorded peak strains. Peak strains may be affected due to variations in ambient temperature and humidity, tire load fluctuations, tire contact pressure and area, noise in the sensor response, and signal sampling errors (Brill et. al. 2009). Theoretically, this value cannot exceed 50% because it would mean that stresses in the unloaded slab exceed stresses in the loaded slab. However, values over 50% for LTE (S) can be attributed to slab curling effects, rounding off error in the data synchronization process, and non-uniformity in pavement properties throughout the test sections (Wadkar, 2010).

3.3 Deflection based LTE using HWD analysis

HWD testing was conducted at the NAPTF using KUAB 240 model between March – April 2004. Testing was carried out at longitudinal joints, transverse joints and slab center locations. A plate of diameter 12 in. and 3 drops of 12,000, 24,000 and 36,000 lbs were used for testing at each location. The objectives of these tests were:

a) Back-calculate layer properties;

b) Verify the uniformity of test items and establish a base line for monitoring performance;

c) Correlate responses under FWD and wheel load;

d) Check joint load transfer capabilities.

The analysis presented in this research is only limited to calculation of LTE (δ) for MRC, MRG and MRS test sections using the loaded and unloaded deflections obtained from HWD sensors across the transverse joints. The highest magnitude of load is used for this analysis. The drop locations are denoted by slab number and direction of load transfer: East to West (E to W) or West to East (W to E). For example, 8 / (W to E) indicate that the load is dropped at the center of transverse joint on slab number 8 with load transferred to slab number 9 (refer to Figure 3 for slab numbers). Tables 11, 12 and 13 summarize the loaded and unloaded deflections with LTE (δ) for MRC, MRG and MRS respectively.

Table 11: Results of HWD data analysis for test item MRC

Drop Location	Drop weight (lbs)	Loaded Deflection (mils)	Unloaded Deflection (mils)	LTE (δ)
10 / (E to W)	36821	14.54	12.04	0.83
9 / (W to E)	37066	14.48	12.56	0.86
9 / (E to W)	36859	15.3	12.57	0.82
8 / (W to E)	36732	15.85	12.99	0.82
8 / (E to W)	36770	15.19	11.74	0.77
7 / (W to E)	36872	15.25	12.1	0.79
7 / (E to W)	36795	15.3	12.18	0.79
6 / (W to E)	36884	14.7	12.56	0.85
15 / (E to W)	37164	15.36	12.15	0.79
14 / (W to E)	37075	14.7	12.83	0.87
14 / (E to W)	37037	15.47	11.99	0.76
13 / (W to E)	37126	15.08	12.45	0.83
13 / (E to W)	37241	15.36	12.57	0.82
12 / (W to E)	37164	14.92	13.15	0.88
12 / (E to W)	36859	16.89	13.04	0.77
11 / (W to E)	36795	17.22	13.15	0.76

Table 12: Results of HWD data analysis for test item MRG

Drop Location	Drop weight (lbs)	Loaded Deflection (mils)	Unloaded Deflection (mils)	LTE (δ)
30 / (E to W)	36974	11.3	9.31	0.82
29 / (W to E)	36910	11.41	9.99	0.88
29 / (E to W)	36897	11.41	9.61	0.84
28 / (W to E)	36884	11.3	9.94	0.88
28 / (E to W)	36961	11.3	9.53	0.84
27 / (W to E)	37025	11.13	9.99	0.9
27 / (E to W)	37063	11.19	9.67	0.86
26 / (W to E)	37025	11.35	10.13	0.89
35 / (E to W)	37509	12.45	10.69	0.86
34 / (W to E)	37305	12.62	10.78	0.85
34 / (E to W)	37292	12.12	9.56	0.79
33 / (W to E)	37253	12.01	10.53	0.88
33 / (E to W)	37356	11.24	9.86	0.88
32 / (W to E)	37202	11.74	9.97	0.85
32 / (E to W)	37228	11.9	10.14	0.85
31 / (W to E)	37190	11.96	10.61	0.89

Table 13: Results of HWD data analysis for test item MRS

Drop Location	Drop weight (lbs)	Loaded Deflection (mils)	Unloaded Deflection (mils)	LTE (δ)
50 / (E to W)	36425	12.29	8.34	0.68
49 / (W to E)	36361	13	8.78	0.68
49 / (E to W)	36208	12.45	9.06	0.73
48 / (W to E)	36527	12.95	8.16	0.63
48 / (E to W)	36451	11.63	8.92	0.77
47 / (W to E)	36489	12.34	8.83	0.72
47 / (E to W)	36540	13.49	8.09	0.6
46 / (W to E)	36387	13.33	9.16	0.69
55 / (E to W)	36451	11.74	7.98	0.68
54 / (W to E)	36515	11.57	8.34	0.72
54 / (E to W)	36541	11.85	8.76	0.74
53 / (W to E)	36451	12.4	8.83	0.71
53 / (E to W)	36413	11.85	8.59	0.72
52 / (W to E)	36451	11.63	9.48	0.82
52 / (E to W)	36337	13.22	8.53	0.65
51 / (W to E)	36464	13.71	9.1	0.66

The average deflection based load transfer efficiency for transverse joints for MRC, MRG and MRS sections for CC2 test pavements is 0.81, 0.86 and 0.70 respectively. The sections with stronger sub-structure or base layer yield lower deflections under FWD loads and in effect show lower LTE (δ) values.

3.3 Summary

The data from concrete strain gage sensors embedded in CC2 test sections on either side of the joints were analyzed. The LTE (S) values at the joints for the first 20 'Go' and 'Return' passes under NAPTV loading are determined using the strain profiles. It is observed that the LTE (S) values under dynamic NAPTV loading for all the three sections are in the range of 0.40 to 0.55. The LTE (S) values greater than 0.50 can be attributed to noise in the strain sensors or error in data synchronization. The average LTE (δ) values for MRC, MRG and MRS test sections were computed using the HWD data.

Chapter 4

Stress-based LTE under static loading

4.1 3D FE modeling using FEAFAA

The FAA has developed a 3D finite element program called FEAFAA (**F**inite **E**lement **A**nalysis - **FAA**) for analysis of multiple-slab rigid airport pavements and overlays. FEAFAA is useful for computing stresses, strains and deflections of rigid pavement structures under aircraft landing gear loads. FEAFAA's basic element type is an eight-node hexahedral (brick) solid element. The model uses only one element type for all structural layers. The bottommost layer of elements in the subgrade consists of 8-noded "infinite" elements. However, infinite elements have special mapping functions that mathematically map the 8-node geometry onto a semi-infinite space. In this way, the FEAFAA model represents a rigid pavement structure on an infinitely deep foundation. A unidirectional spring element is used for modeling linear elastic joints between adjacent slabs. In FEAFAA, the joints act as continuous, linear elastic springs, transmitting vertical loads between adjacent slabs in shear through the joint. The latest version, FEAFAA 2.0, is obtained from the FAA which enables the user to vary the temperature gradient at the top and bottom of the slab. Pavement responses under static aircraft loading and subjected to temperature gradients can be obtained using this version. The MRC, MRG and MRS sections of CC2 test pavement are modeled using FEAFAA 2.0 for this study.

4.2 Sensitivity analysis

Using the latest version of FEAFAA, a sensitivity analysis is carried out to study the impact of concrete and base properties of the pavement on static stress based load transfer efficiency of the

three CC2 test sections. The FEAFAA model is also used analyze the sensitivity of static LTE (S) to airplane loading and configurations, temperature curling and pavement joint stiffness.

4.2.1 Effect of Concrete properties on LTE (S)

The FEAFAA program is used to study the impact of the modulus of elasticity of the PCC layer on stress based load transfer efficiency. FEAFAA allows the user to select a PCC modulus in the range of 5 million psi to 8 million psi. A 2-slab model with 12 in. thick PCC layer and base and subgrade properties similar to MRC test section is used. A single wheel aircraft, SWL-50, with an edge loading case is used for the analysis. The joints are modeled using dowels of diameter 1.0 in. with spacing of 12.0 in. For the above doweled joint configuration, the default equivalent joint stiffness value in FEAFAA is 143 ksi.

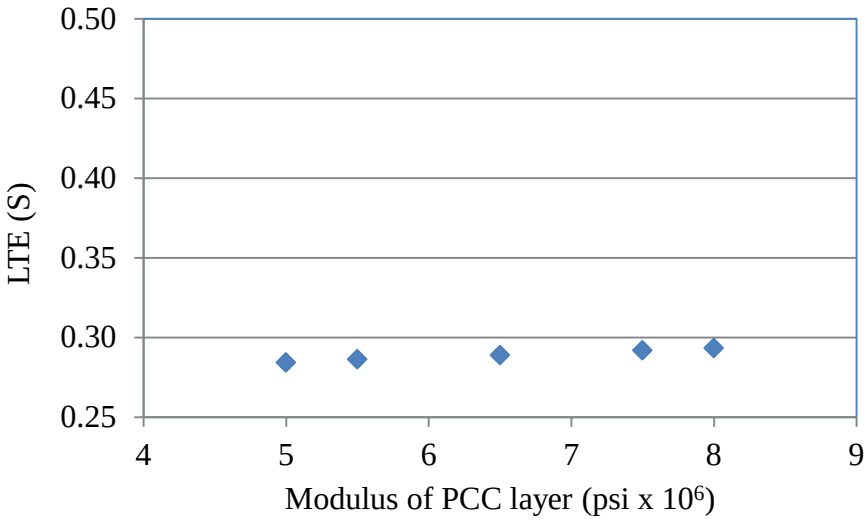

Figure 10: Effect of modulus of PCC layer on LTE (S)

The results show that, the stress base load transfer efficiency is not sensitive to surface layer modulus of elasticity. An increase in PCC modulus from 5 million psi to 8 million psi causes the LTE (S) value to increase by 0.009 which is negligible.

4.2.2 Effect of base properties on LTE (S)

A 2-slab model was analyzed using FEAFAA to study the effect of modulus of base layer on the stress-based LTE. The concrete and subgrade layer properties were kept constant similar to the MRC section of the CC2 test pavement. The layer thickness of each of the pavement layers is kept constant and only the modulus of base is varied from 30,000 psi to 500,000 psi. The slabs are loaded using a single wheel aircraft at the joint and the LTE (S) is calculated using the stresses at the loaded and unloaded slabs. Figure 11 shows the sensitivity of LTE (S) to the modulus of base.

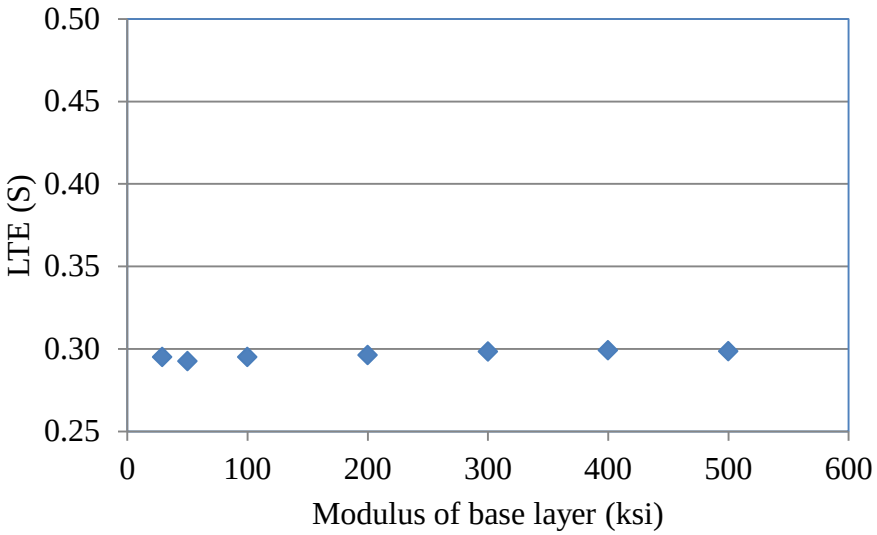

Figure 11: Effect of modulus of base layer on LTE (S)

It is observed that LTE (S) is not sensitive to the modulus of elasticity of the base layer. As seen from the figure, the LTE (S) remains in the range of 0.29 to 0.30 for varying modulus of base layer.

4.2.3 Effect of Airplane gear configuration on LTE (S)

The impact of airplane gear configuration on LTE (S) was studied using FEAFAA. A 2-slab model was loaded at the joint with different aircraft gear configurations keeping the airplane gross weight constant at 400,000 lbs. Four types of airplanes: Sngl Whl-75; Dual Whl-75, Dual Tan-100 and A-380-800 were used to study the effect of different aircraft gear configuration on LTE (S). The gear orientation is parallel to the longitudinal joint. The geometric characteristics of the aircrafts used in this analysis are given in table 14.

Table 14: Geometric characteristics of aircrafts

	Sngl Whl-75	**Dual Whl-75**	**Dual Tan-100**	**A-380-800**
Number of Wheels	1	2	4	6
Dual spacing (in.)	0.0	21.0	20.0	53.1
Tandem spacing (in.)	0.0	0.0	45.0	66.9
Wheel load (lbs.)	400,000	200,000	100,000	666,66.7
Tire Pressure (psi)	400	400	200	200

This analysis was carried out for MRG, MRC and MRS test sections of CC2. The findings from this analysis are represented using Figure 12.

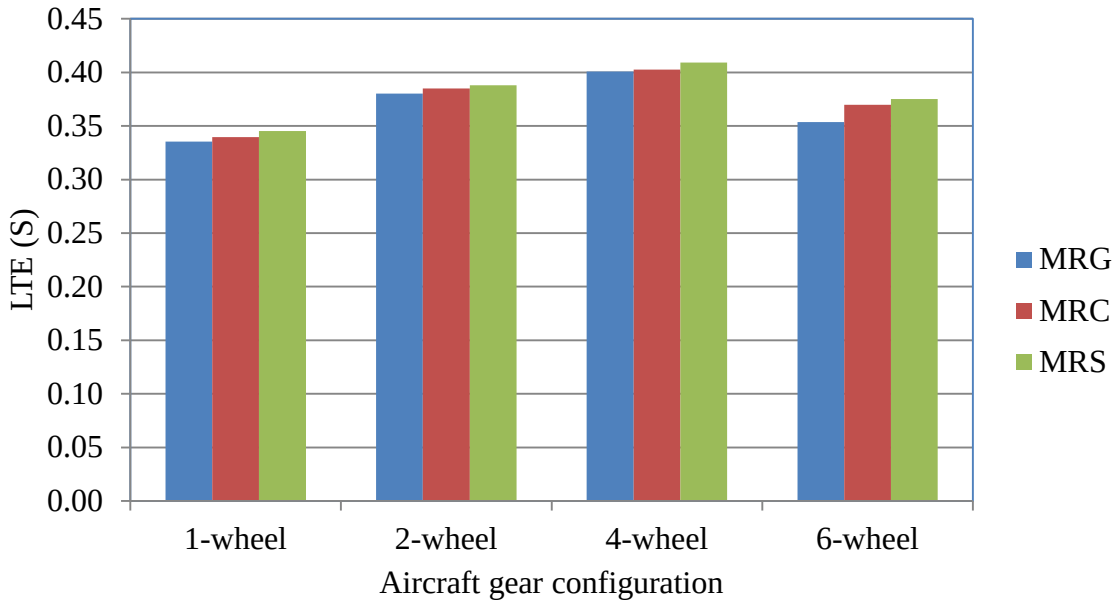

Figure 12: Effect of aircraft gear configuration on LTE (S)

The analysis shows that MRS section exhibits the highest LTE (S) value irrespective of the airplane wheel configuration. However the LTE (S) of a particular pavement structure varies with the airplane wheel configuration. The results show that the LTE (S) increases by about 13% as the wheel configuration changes from single wheel to dual wheel, about 16% as the wheel configuration changes from single wheel to dual tandem and around 6% as the wheel configuration changes from single wheel to 3 duals in tandem (6-wheel). The LTE (S) shows an increasing trend as the number of wheels increase from single wheel to dual tandem but shows a decreasing trend as the number of wheels increase beyond four.

4.2.4 Influence of temperature gradient on stress at the joint

A two slab model was analyzed using FEAFAA to study the effect of varying temperature gradients on stresses at the joint. The slab thickness for MRG, MRC and MRS are kept constant at 12 in. The single wheel aircraft load is located at the edge of the slab and is kept constant at 50,000 lbs. The joints are modeled using an equivalent shear stiffness chosen to represent dowels of diameter 1.0 in. with spacing of 12.0 in. For the above doweled joint configuration, the default equivalent joint stiffness value in FEAFAA is 131 ksi. The temperature at the top of the slab is kept constant at 0^{o}F while the temperature at the bottom is varied from 12^{o}F to -12^{o}F. FEAFAA assumes that the temperature is linearly distributed through the thickness of the slab. The positive gradient is when the temperature at the top is lower than the bottom of the slab and negative gradient is when the surface temperature is higher than the bottom of the slab.

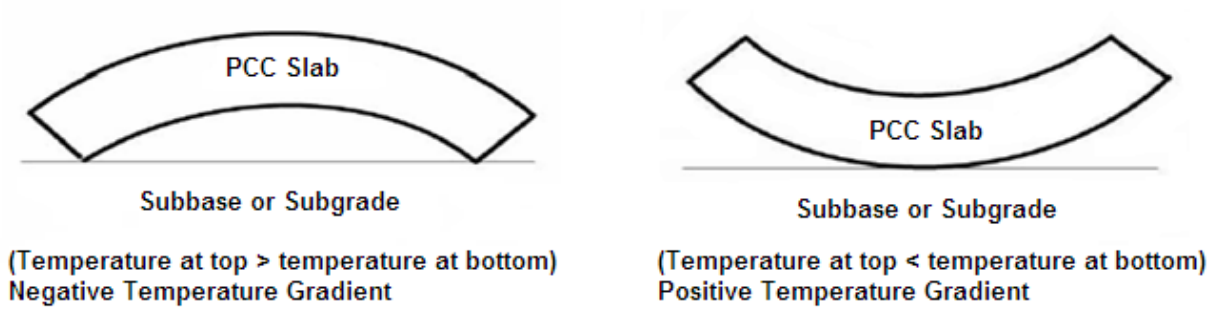

Figure 13: Slab curling due to temperature gradient

The stresses at the joint are calculated under varying temperature gradients. Figure 14 shows the sensitivity of temperature gradients on stress at the joint for MRG, MRC and MRS sections.

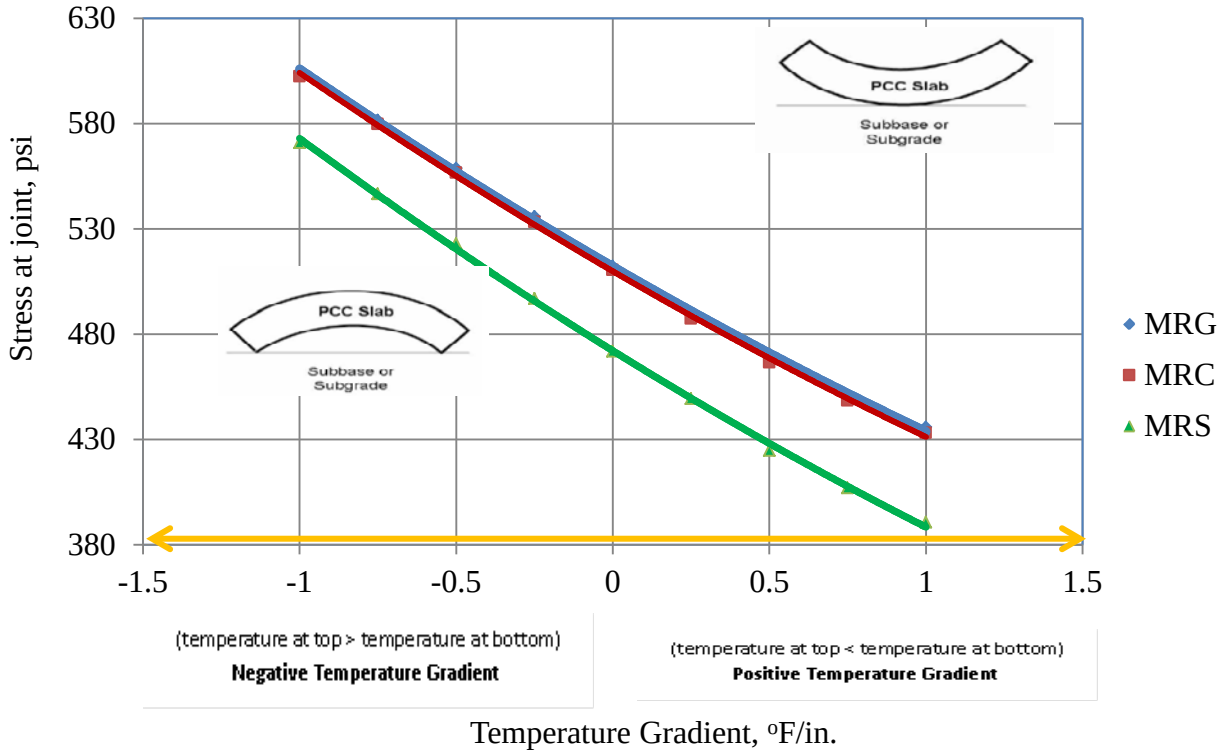

Figure 14: Temperature gradient versus stresses at the joint for MRG, MRC and MRS sections

Figure 14 indicates that stresses at the joint decrease with increasing temperature gradients. For a constant load of 50,000 lbs, the joint stresses in MRG, MRC and MRS decrease by 168.2 psi, 169.2 psi and 180.2 psi respectively for an increase in temperature gradient from -1°F/in. to 1°F/in. The section with stronger sub-structure yields lower stresses at the joint and shows higher reduction in stresses with increase in temperature gradient.

4.2.5 Effect of temperature curling on LTE (S)

A sensitivity analysis of temperature gradient to LTE (S) for MRG, MRC and MRS test items is carried out using FEAFAA. In this analysis the aircraft gross weight was kept constant at 50,000 lbs, and the temperature gradient increment is 0.25 ^{0}F/in. The equivalent joint stiffness was once again kept at a default value of 131 ksi. The stresses were calculated at the loaded and unloaded slabs at the joint and a graph of LTE (S) vs. temperature gradient is plotted as shown in Figure 15.

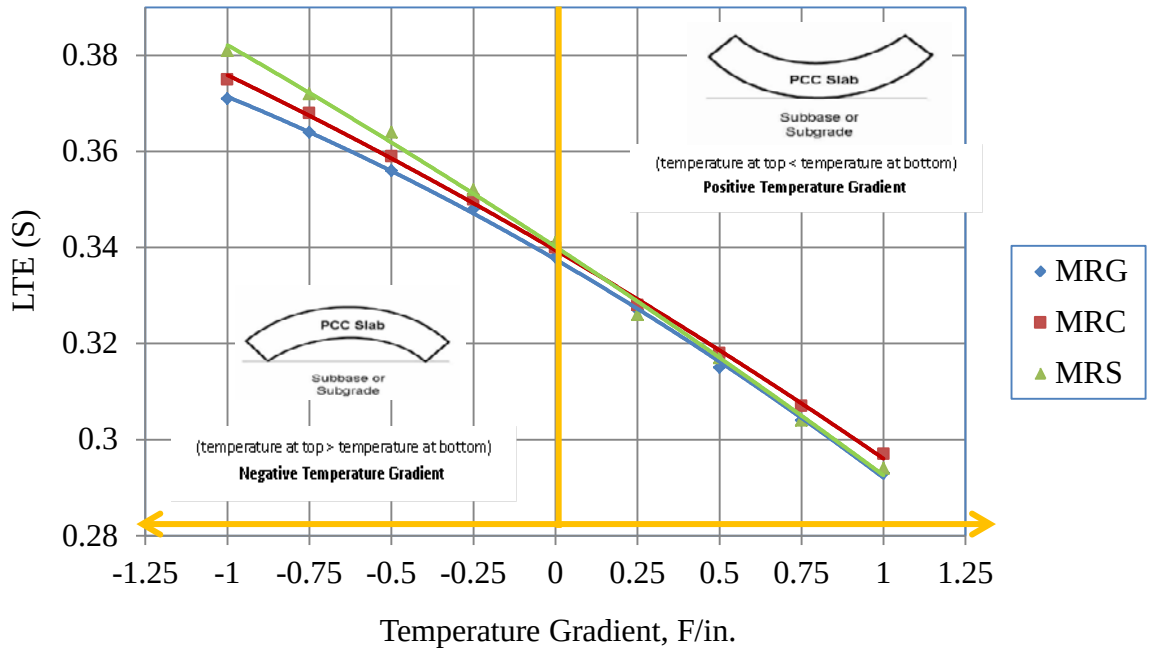

Figure 15: LTE (S) versus temperature gradient for MRG, MRC and MRS sections

At 0^{o}F/in. temperature gradient, the LTE (S) of all the pavement sections is about 0.34. For all the three sections, it is observed that the LTE (S) increases as the temperature gradient decreases. The average increase in LTE (S) is 0.039, 0.039 and 0.0435 for MRG, MRC and MRS sections

respectively for every 1^{o}F/in. drop in the temperature gradient. MRG, MRC and MRS sections exhibit fairly similar LTE(S) values with varying temperature gradient. This indicates that the influence of temperature gradient on LTE(S) is independent of sub-structure layer properties and thicknesses. It is important to note that the change in LTE (S) depends not only on the temperature gradient, but also the load.

4.2.6 Effect of joint stiffness on LTE (S)

Stress-based LTE is calculated under varying joint stiffness using the FEAFAA model. The joint stiffness for all the three sections, MRG, MRC and MRS was varied in FEAFAA to represent a range of spacing between the dowel bars. The effective joint stiffness was varied from 87,500 psi to 262,500 psi to represent dowel bar spacing from 18 in. to 6 in. Figure 16 shows the sensitivity of LTE (S) to joint stiffness.

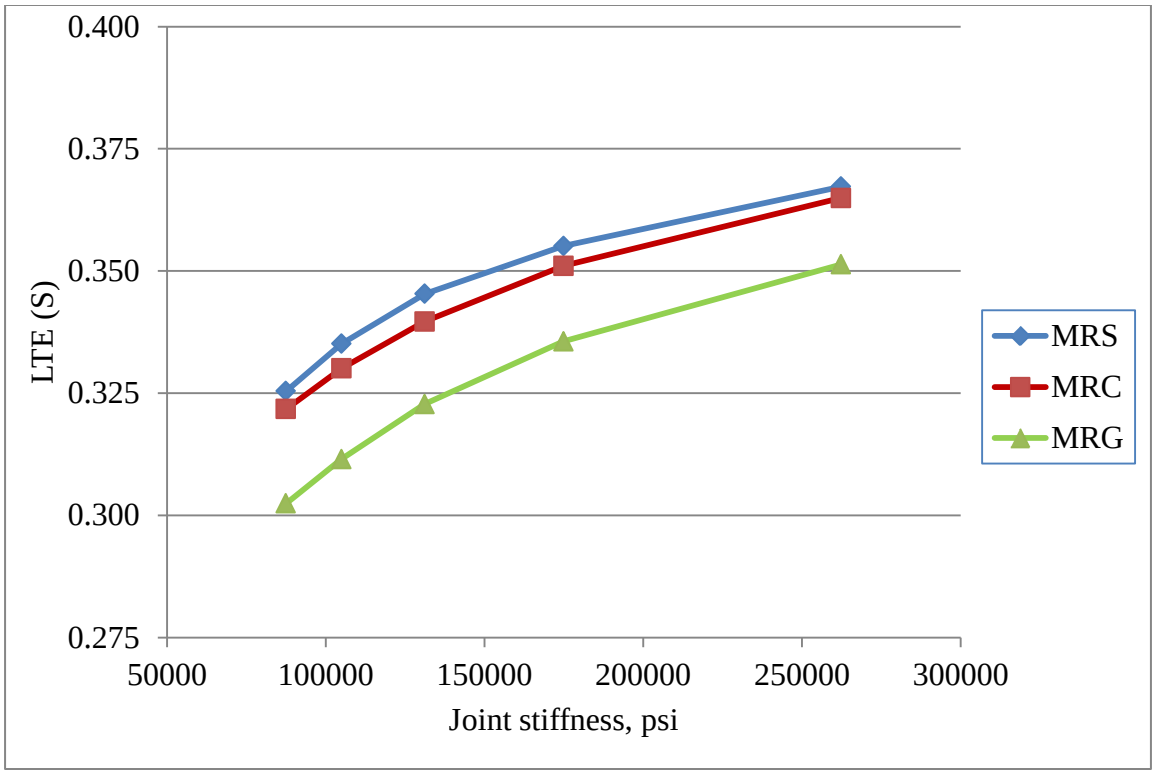

Figure 16: Effect of joint stiffness on LTE (S)

It is observed that, for a given loading and joint stiffness value, MRS section exhibits the highest LTE (S) followed by MRC and MRG. The analysis indicates that LTE (S) of a weaker sub-structure is more sensitive to joint stiffness than stronger sub-structures. When the stiffness at the joint is increased from 87,500 psi to 262,500 psi, the LTE (S) increases by 0.049, 0.043 and 0.042 for MRG, MRC and MRS sections respectively.

4.3 Summary

A 3D finite element program, FEAFAA, was used to model the MRG, MRC and MRS sections of the CC2 test pavement. A sensitivity analysis is carried out to study the impact of concrete and base properties of the pavement on LTE (S). The impact of temperature gradient between

the top and bottom of the PCC slab on critical edge stresses and LTE (S) is analyzed. Finally, the effect of joint stiffness on LTE (S) is analyzed. The findings indicate that LTE (S) is insensitive to modulus of base layer and slightly sensitive to PCC layer modulus and aircraft loading configuration. The temperature gradient has a considerable impact on the LTE (S) and critical tensile stresses at the joint. The stress based load transfer efficiency is highly sensitive to joint stiffness.

Chapter 5

Stress-based dynamic LTE under moving aircraft

5.1 3D FE modeling using ABAQUS

ABAQUS is a general-purpose, commercial, nonlinear finite element code, which is used in many engineering fields. This software provides numerous interactions, constraints, mesh generators, and different loading conditions which make it suitable to carry out a complicated dynamic analysis. ABAQUS version 6.10 was used to perform dynamic analysis of rigid pavement. The concrete slab is characterized by modulus of elasticity, Poisson's ratio and pavement damping coefficient while the foundation is characterized by a modulus of subgrade reaction and foundation damping coefficient. Creating a realistic model and calibration of model parameters is necessary for obtaining accurate dynamic and damping behavior of rigid pavements. To obtain correct model parameters such as element type, mesh size, interactions between foundation layers, boundary conditions, joint stiffness value and damping parameters, a series of steps were performed.

Element Type and Mesh Size – A simply supported concrete beam with concentrated loading at the center was modeled using ABAQUS. The deflections and stresses were obtained at the center of the beam under varying element types and mesh sizes. The results were compared with available closed form solutions which are given as follows:

$$\text{Max. Displacement at the bottom of beam: } \Delta = \frac{PL^3}{48EI} \tag{14}$$

$$\text{Max. Stress in X – direction: } \sigma = \left(\frac{PL}{4}\right)\left(\frac{y}{I}\right) \tag{15}$$

Where,

Δ = maximum deflection, (ft.)

P = total load, (lbf)

L = span of the beam, (ft.)

I = Moment of Inertia, (ft^4)

E = elastic modulus of slab, (psf)

σ = Max. stress in X direction, (psf)

y = distance between centroid and bottom edge of the beam, (ft.)

The beam dimensions and properties are given in Table 15. The stresses and deflections are obtained under varying mesh sizes for comparison (Table 16).

Table 15: Beam dimensions and properties

Dimensions		
X (ft.)	Y (ft.)	Z (ft.)
20	2	1
Properties		
Density (lb/ft^3)		150
Young's Modulus (psf)		936000000
Poisson's Ratio		0.15
Concentrated Load at the center (lbf)		200

Table 16: Stresses and Deflections under varying mesh size

Element Type - C3D8R An 8-node linear brick, reduced integration, hourglass control.							
Beam Size (ft.xft.)	**Mesh Size (ft.xft.)**	**Closed Form Stress (psf)**	**FEM Stress (psf)**	**% Error**	**Closed Form Deflection (ft.)**	**FEM Deflection (ft.)**	**% Error**
20X2	0.4X0.4	1500	1240	17.3	5.64E-05	5.79E-05	2.59
20X2	0.25X0.25	1500	1370	8.9	5.64E-05	5.72E-05	1.41
20X2	0.2X0.2	1500	1440	4.33	5.64E-05	5.66E-05	0.3
20X2	0.165X0.165	1500	1510	0.87	5.64E-05	5.63E-05	0.25

It is observed that for C3D8R reduced integration element, the stresses and deflections are within 1% error if ratio of element size to beam dimensions is approximately 1:1500.

ABAQUS results matched closely with that of closed form solutions for simply supported beam model and hence the model is expanded to a simply supported slab. The formulae for flat plates with straight boundaries and constant thickness were used to calculate stresses and deflections. For uniform load over the entire slab, equations 16 and 17 are used (Theory of Elastic Stability, 2nd edition, 1963).

$$\text{Maximum deflection: } \Delta = -\frac{\alpha q b^4}{E t^3} \tag{16}$$

$$\text{Maximum stress at center of slab: } \sigma = \frac{\beta q b^2}{t^2} \tag{17}$$

Where,

q = uniform load on slab, (psf)

t = slab thickness, (ft.)

a = length of slab (m); b = width of slab, (ft.)

α, β = constants depending on b/a ratio

E = elastic modulus of slab, (psf)

The stresses and deflections observed were noted and compared against calculated values. The simply supported condition was simulated by constraining the bottom edges of the slab in Z direction.

Table 17: Slab dimensions and properties

Case	b/a	a (ft)	b (ft)	U	α	β	E (psf)	t (ft)	q (psf)
1	1	8	26	0.3	0.0444	0.2874	501250	0.35	0.21
2	1.2	8	22	0.3	0.0616	0.3762	501250	0.35	0.21
3	1.4	8	19	0.3	0.077	0.453	501250	0.35	0.21

ABAQUS results for case 1 were obtained using C3D8R - reduced integration and C3D8I – Incompatible elements for varying element sizes.

Table 18: Stresses and Deflections under varying Mesh Size and Element Type

Element Type - C3D8R An 8-node linear brick, reduced integration, hourglass control.						
Element Size (ft.xft.)	**Closed Form Stress (psf)**	**FEM Stress (psf)**	**% Error**	**Closed Form Deflection (ft.)**	**FEM Deflection (ft.)**	**% Error**
0.05	1.50E+03	1.36E+03	9.56	-1.77E-03	-1.91E-03	-7.96
0.1	1.50E+03	1.16E+03	22.74	-1.77E-03	-2.09E-03	-18.20
0.2	1.50E+03	1.02E+03	31.87	-1.77E-03	-2.45E-03	-38.85
0.3	1.50E+03	6.48E+01	95.68	-1.77E-03	-1.58E-01	-8828.52
Element Type - C3D8I An 8-node linear brick, incompatible modes						
Element Size (ft.xft.)	**Closed Form Stress (psf)**	**FEM Stress (psf)**	**% Error**	**Closed Form Deflection (ft.)**	**FEM Deflection (ft.)**	**% Error**
0.3	1.50E+03	1.53E+03	-1.63	-1.77E-03	-1.82E-03	-3.20
0.4	1.50E+03	1.52E+03	-1.36	-1.77E-03	-1.82E-03	-3.09
0.5	1.50E+03	1.51E+03	-0.76	-1.77E-03	-1.82E-03	-2.69
0.6	1.50E+03	1.49E+03	0.90	-1.77E-03	-1.78E-03	-0.88
0.7	1.50E+03	1.47E+03	2.10	-1.77E-03	-1.77E-03	0.13

The results obtained from the above analysis show that brick elements with incompatible modes can be efficiently used. The basic quadrilateral linear elements were modified by adding quadratic modes of deformation by Wilson et. al. in 1973 to reduce spurious shear deformations and to improve the representation of bending in the interior of the element. These elements are referred as 'incompatible' or 'non-conforming' as the additional modes break the continuity across element boundaries except at the nodes themselves (Hughes, 1987). These elements provide better bending behavior as the modes eliminate the stiffening effect introduced due to shear stresses and Poisson's ratio (ABAQUS user manual). The incompatible elements give better results than the reduced integration elements for coarser element sizes thereby reducing the computation time. The stresses and deflections are within 1% error if ratio of element size to beam dimensions is approximately 1:180.

Using incompatible elements and optimum mesh size the results were obtained for all the cases stated in Table 18 above.

Table 19: Stresses and Deflections for a Simply Supported Slab

Element Type - C3D8I An 8-node linear brick, incompatible modes						
Case	**Closed Form Stress (psf)**	**FEM Stress (psf)**	**% Error**	**Closed Form Deflection (ft.)**	**FEM Deflection (ft.)**	**% Error**
1	1.50E+03	1.49E+03	0.90	-1.77E-03	-1.78E-03	-0.88
2	1.36E+03	1.35E+03	1.24	-1.77E-03	-1.20E-03	-1.06
3	1.21E+03	1.20E+03	0.62	-1.77E-03	-8.18E-04	-2.50

The findings show that ABAQUS results using C3D8I elements and relatively coarser mesh sizes for simply supported slab match with the analytical solutions.

Interactions between foundation layers - Analytical solutions based on Westergaard's work were also used to compare FE-based model predictions for multi-layered pavements. Westergaard developed analytical solutions for a single large slab under circular loaded area. The slab is assumed to be elastic with constant thickness, modulus of elasticity and Poisson's ratio. The stress (σ) and deflection (Δ) for a point located at the bottom of the slab directly under the center of a loaded circular area are given by equations 18 and 19 (Pavement Analysis & Design, 2nd edition, 2004).

For interior loading,

$$\text{Maximum Stress: } \sigma = \frac{3P}{2\pi h^2}(1+\mu)\{\ln\left(\frac{l}{b}\right) + \frac{\ln[12(1-\mu^2)]}{4}\} \quad (18)$$

$$\text{Maximum Deflection: } \Delta = \frac{P}{8kl^2}[1 - \frac{1}{2\pi}(\frac{a}{l})^2\{\ln\left(\frac{l}{b}\right) + \frac{\ln[12(1-\mu^2)]}{4} + 0.75\} \quad (19)$$

Where,

P = total load, (lbf)

h = slab thickness, (ft.)

μ = slab Poisson's ratio,

l = radius of relative stiffness, $l = \sqrt[4]{(\frac{Eh^3}{12(1-\mu^2)k})}$, (ft.)

E = elastic modulus of slab, (psf)

k = modulus of subgrade reaction, (pcf)

$b = a$ if $a = 1.72h$

$= \sqrt{1.6a^2 + h^2} - 0.675h$ if $a < 1.72h$

a = radius of the circular loading area, (ft.)

The base and subgrade are modeled in ABAQUS as linearly elastic with modulus of elasticity and Poisson's ratio as input parameters.

MRC section of CC2 test pavement is modeled for verification of interaction properties used between the layers in ABAQUS model.

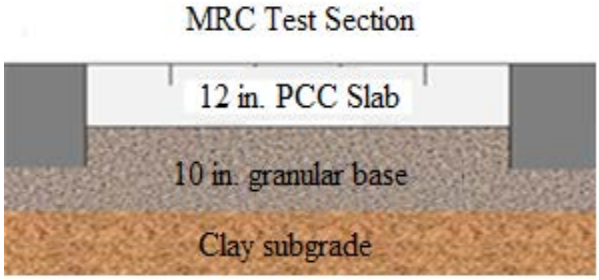

Figure 17: MRC sectional view

The material properties for the MRC CC2 section were obtained from the NAPTF database and are given in Table 20.

Table 20: CC2 Model Properties

Layer	**Thickness (in.)**	**Modulus of Elasticity (psi)**	**Density (pcf)**	**Poisson's Ratio**
PCC Slab (6 Slab model)	12	$6.5X10^6$	150	0.15
Aggregate Base Course	10	29,000	160	0.4
Clay Subgrade	240	10,500	110	0.45

C3D8I elements were used for modeling. The interaction between the surfaces of the layers is modeled using surface to surface hard contact property available in ABAQUS. The boundary conditions are similar to previously modeled single slab model. The equivalent k-value for CC2 MRC foundation section was calculated using the above properties and was found to be 142 psi/in (244,616 pcf). The model was subjected to interior circular loading with plate radius of 1.2 ft. The thickness and modulus of PCC layer is kept constant at 1 ft. and 936 million psf respectively. The Poisson's ratio of the top layer is 0.15. The closed form deflections and stresses given by equations 18 and 19 were compared against FEM deflections and stresses. The results are given in Table 21.

Table 21: Stresses and deflections for a Slab resting on Layered Foundation

Case	p (psf)	l (ft)	b (ft)	Calculated σ (psf)	FEM σ (psf)	% error	Calc. Δ (ft.)	FEM Δ (ft.)	% error
1	10800	4.25	1.143	51760	47100	8.96	1.34E-03	1.42E-03	-6.33
2	14400	4.25	1.143	69010	62800	8.96	1.78E-03	1.89E-03	-6.28
3	21600	4.25	1.143	103520	94200	9.04	2.67E-03	2.84E-03	-6.23

It is observed that FEM stresses and deflections match with calculated closed form stresses and deflections with an error of less than 10%.

5.1.1 Calibration of Model Parameters

A 4-slab MRC section is modeled using ABAQUS to determine the joint stiffness and damping values comparable to field conditions. The slabs are connected with springs to simulate dowel

joints. The joint stiffness is adjusted by varying the spring constant 'k_s' for spring elements. ABAQUS provides 'Rayleigh' damping for mode-based (linear) dynamic analysis. Studies have shown that damping in concrete is mainly stiffness proportional and hence mass proportional damping is neglected (Yu et. al., 2010). The model parameters used to replicate the MRC section are given in Table 22.

Table 22: Model parameters used for MRC section

Concrete and Foundation Model	Linear Elastic
Elements	C3D8I - 8-node linear brick, Incompatible modes.
Mesh Size	6in. X 6in. (slab); 12 in. X 12in. (foundation)
Interactions	Surface to Surface Hard Contact
Joint Simulation	Simulated using spring elements
Pavement damping	Stiffness proportional, 'β', s
Foundation damping	Neglected
Loading	HWD / Dynamic
Boundary Conditions	Displacements U_1 and U_2 in base layer are constrained. Subgrade layer is constrained in all directions (U_1, U_2 & U_3) at the bottom.

The spring constant 'k_s' and stiffness proportional damping 'β' values for MRC section are obtained using the field HWD data from NAPTF. HWD impulse loading is simulated in ABAQUS by defining a time-amplitude relation as shown in Figure 18. FEM deflections for 3 different loads at 5 distinct points on the loaded and unloaded slabs are calculated and compared against field HWD data. Figure 19 below shows the location of points D_0 through D_4 where the deflections are measured. D_0 represents the center of the loading plate which is 6 inches away from the joint. Point D_1 is on the unloaded slab while D_0, D_2, D_3 and D_4 are on the loaded slab.

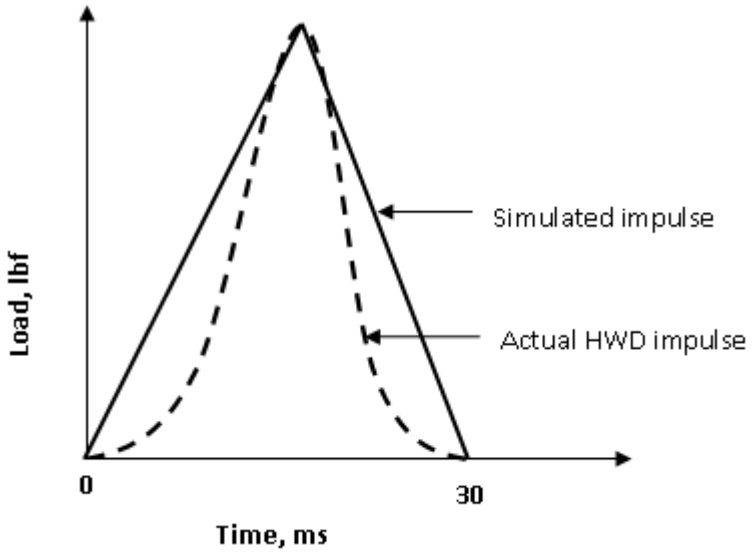

Figure 18: HWD loading impulse

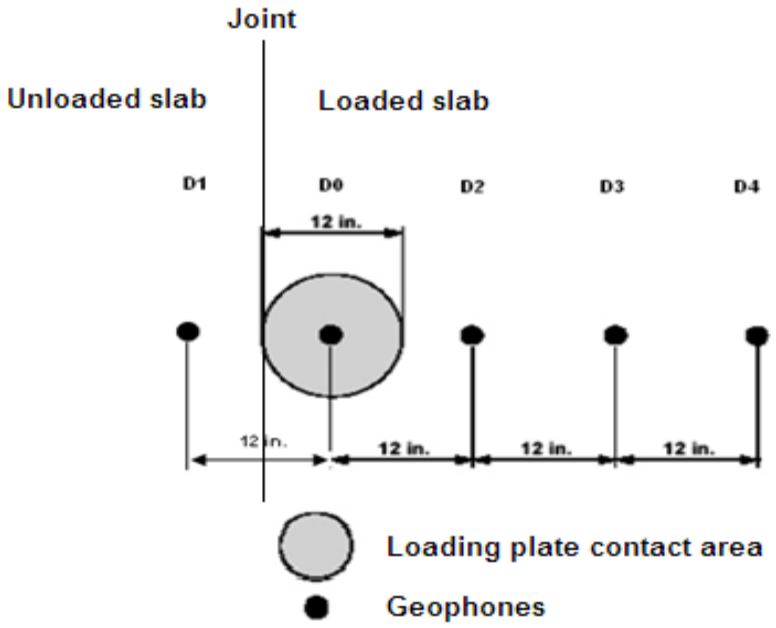

Figure 19: Location of loading wheel and geophones for HWD

The spring constant is adjusted such that the calculated deflection based LTE (δ) is same as the average field measured value of 0.81. The deflection based LTE is defined as the ratio of unloaded versus loaded slab deflection. A spring constant of $2.1X10^8$ lbf/ft. gives the desired deflection based LTE of 0.81. The β value is calibrated to the actual field measured unloaded and loaded HWD deflections. It is observed that the damping value increases with an increase in loading rate. β values of 0.31 s, 0.33 s and 0.35 s are used for HWD loads of 12399 lbs, 24674 lbs and 36732 lbs, respectively to match the FEM predicted deflections. However, a unique relationship may not exist between the damping coefficients and loading. It could depend on several factors, such as structure of the pavement and mechanical properties of individual layers. Figure 20 shows the comparison of calculated deflections from 3D FE analysis with the observed field deflections for three different loads. The error is within 10%.

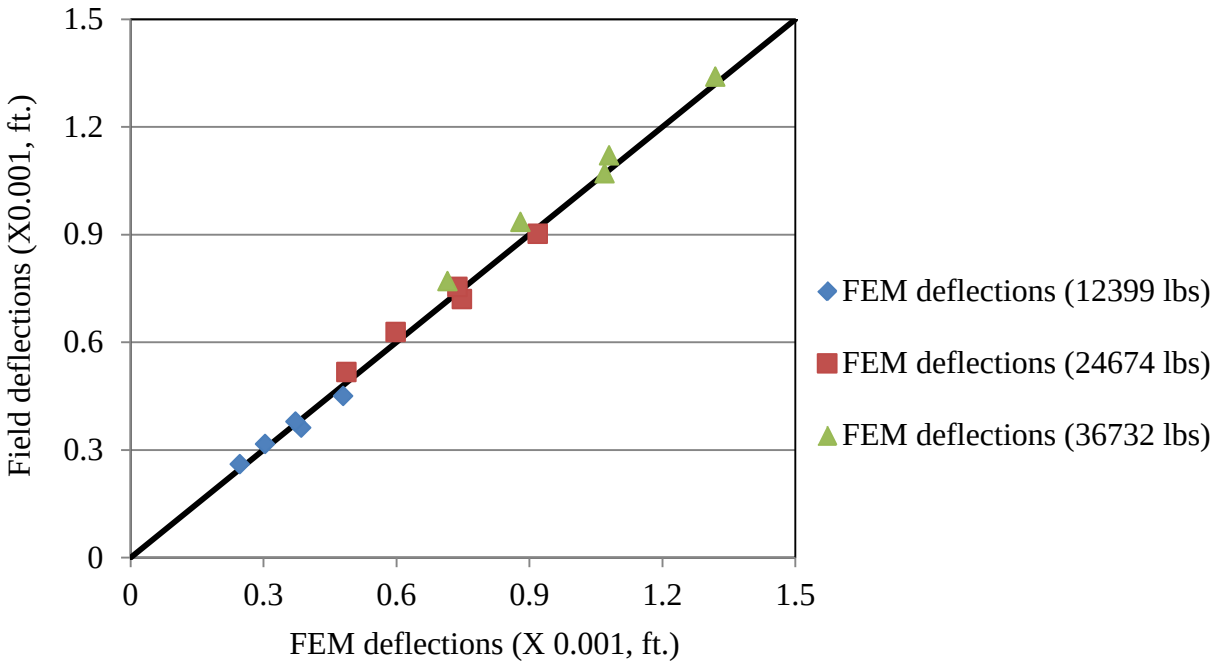

Figure 20: Comparison of FEM deflection with field data

5.1.2 Validation of the Model

Strain response profiles from CSG-5 and CSG-7 sensors are obtained for NAPTV loading at a speed of 3.67 fps (2.5 mph). The nominal load was 55,000 lbs. per wheel at 210 psi tire pressure. The FE predicted dynamic pavement responses are obtained at sensor locations as the NAPTV travels across the joint. The dual tandem wheel configuration of the NAPTV is simulated in ABAQUS by applying the load on a set of elements covering the loaded footprint area. The amplitude of tire pressure acting on each of the elements is varied with time to simulate the movement of NAPTV. The schematic (Figure 21) shows the pressure amplitude on element 4, as the wheel moves from position A to E.

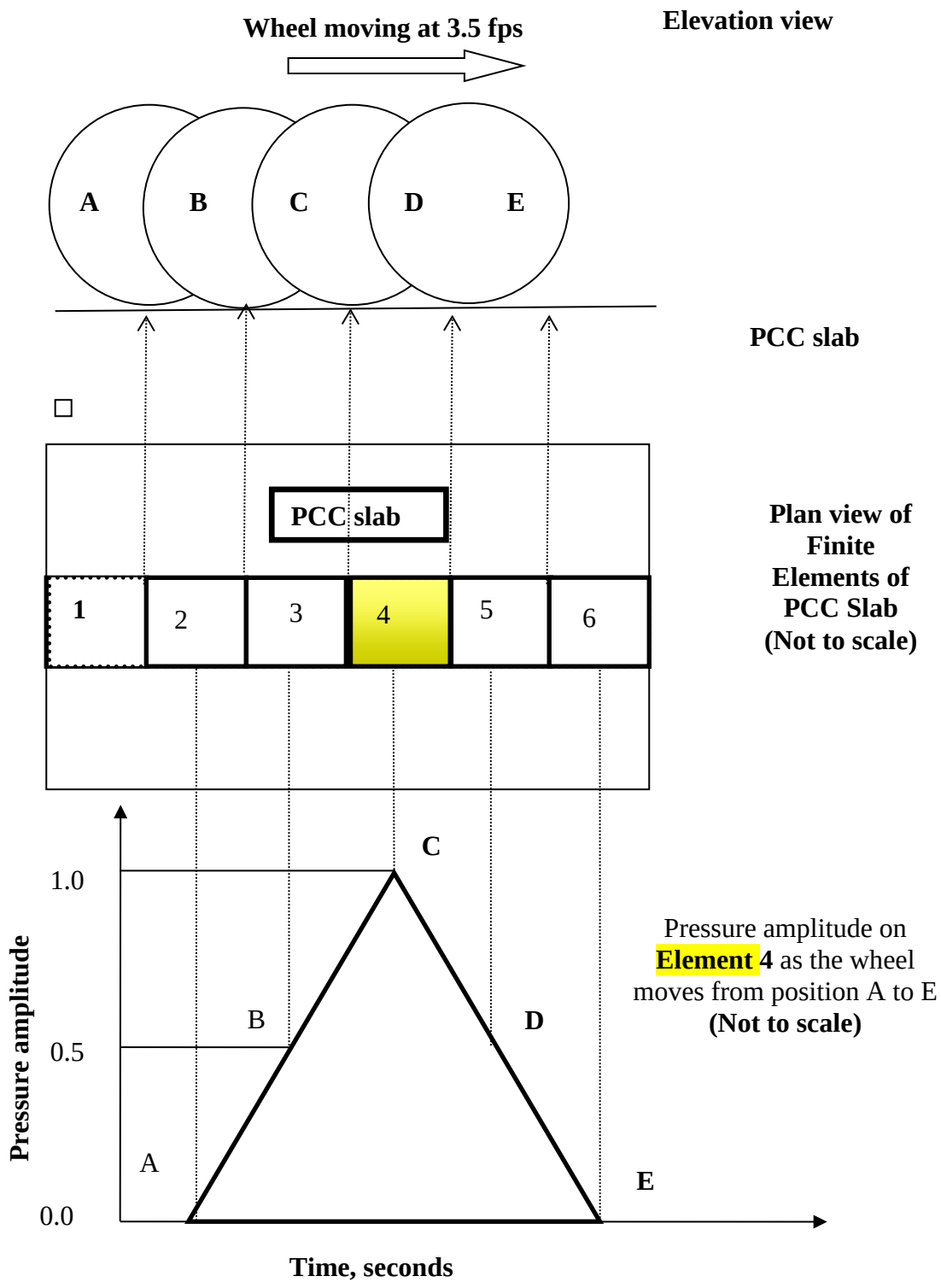

Figure 21: Schematic representation of FEM modeling of moving load

The tire pressure is then applied to adjoining elements as the NAPTV moves forward in the direction of motion. A spring constant of $2.1X10^8$ lbf/ft. and pavement damping corresponding to 'β' of 0.25 s is used. Essentially, the strain gage should exhibit a peak value when the wheels are directly over the strain gage. However, a time lag is observed in the FEM strain predictions as the peak strain occurrence time does not coincide with the time when the aircraft wheels are directly over the sensor. This time lag is due to the effect of pavement inertia and damping (Chatti et. al., 2004).

Figure 22 and 23 show the comparison of FE model predicted strains to field data obtained from sensors CSG-7 and CSG-5. The responses for a Track 0 event wherein the NAPTV wheel passes directly over the sensor CSG-7 is compared to model predicted strains in Figure 22. The error is minimal in the vicinity of the peak. Figure 23 shows the comparison of field responses from CSG-5 to model predicted responses for Track 1, which is 1 ft. to the right of Track 0 (refer to Figure 5). The error in the strain values may be attributed to additional strains developed due to pavement roughness and temperature and moisture curling which are assumed to be zero in the finite element model.

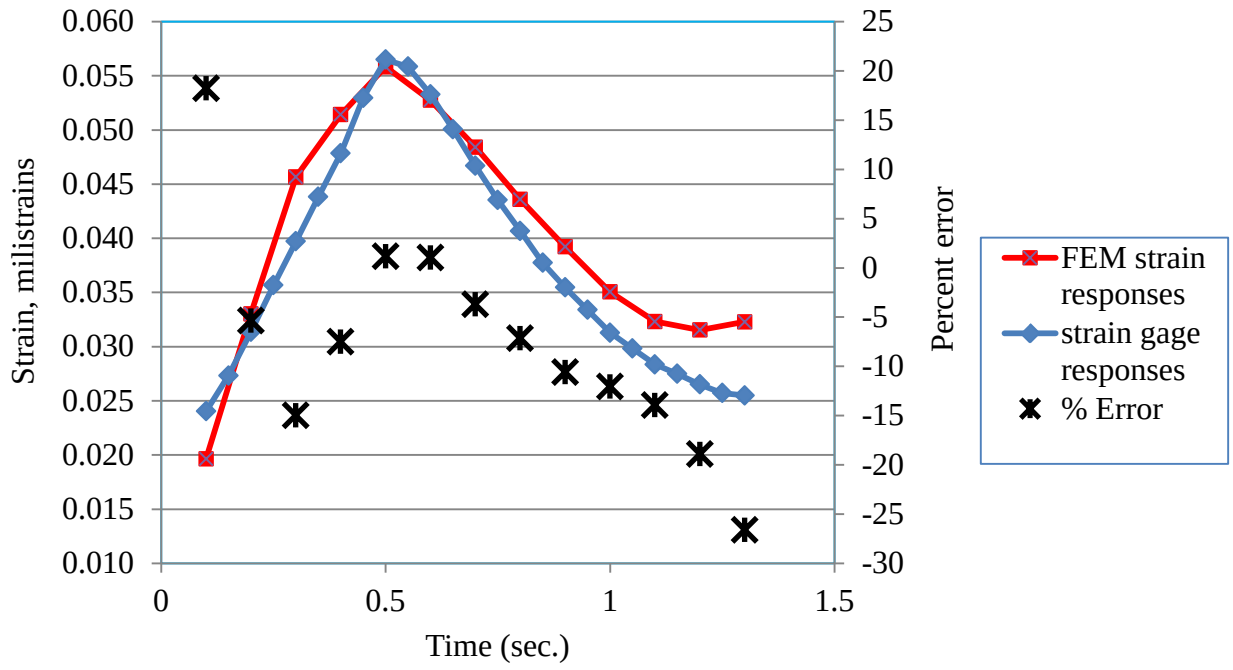

Figure 22: Comparison of predicted FEA strain response with field measured strain gage sensor data for CSG-7 (Track 0 event)

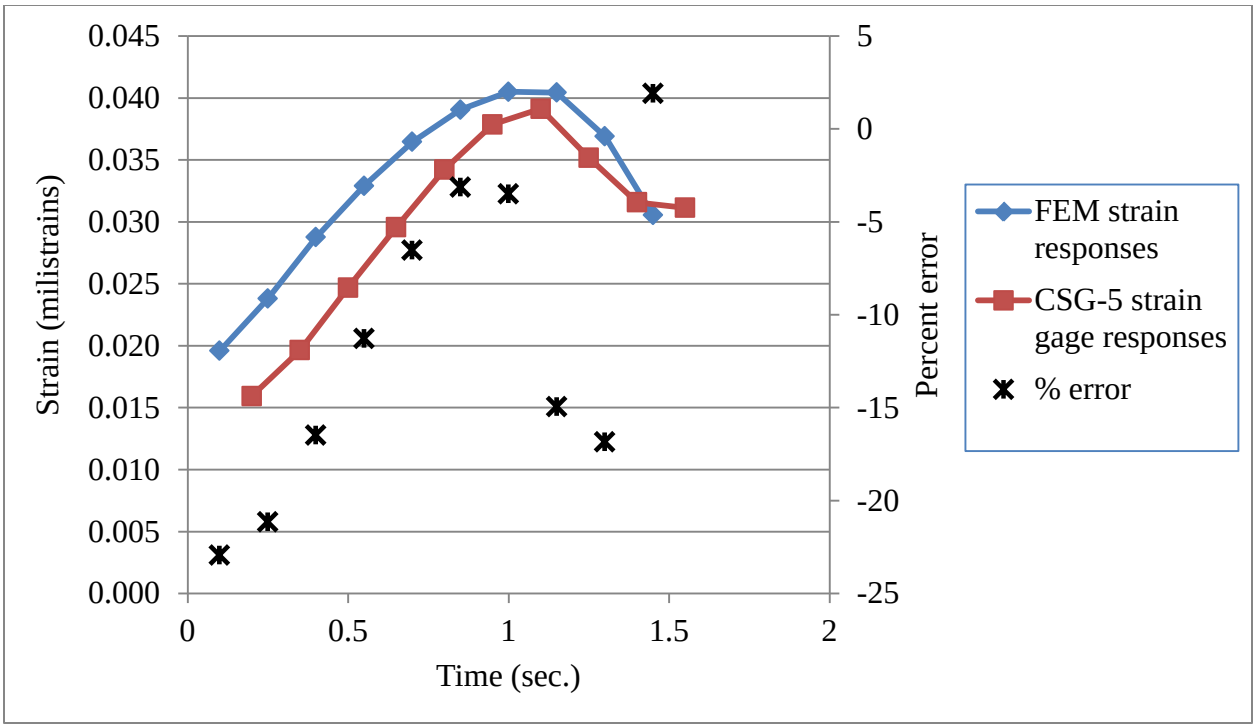

Figure 23: Comparison of predicted FEA strain response with field measured strain gage sensor data for CSG-5 (Track 1 event)

5.2 Sensitivity analysis

The calibrated model parameters and damping values were used to conduct a sensitivity analysis. As the damping value for the pavement may vary with the rate of loading, a range of damping coefficient 'β' values from 0.2 s to 0.6 s are selected for this analysis. The loaded strain (ε_L) and unloaded strain (ε_U) profiles at the joint are obtained from FE analysis under varying aircraft speeds and pavement damping values. Figure 24 shows a typical ε_L and ε_U profile obtained from strain gages for a single wheel aircraft moving with a speed of 3.67 fps under NAPTV loading.

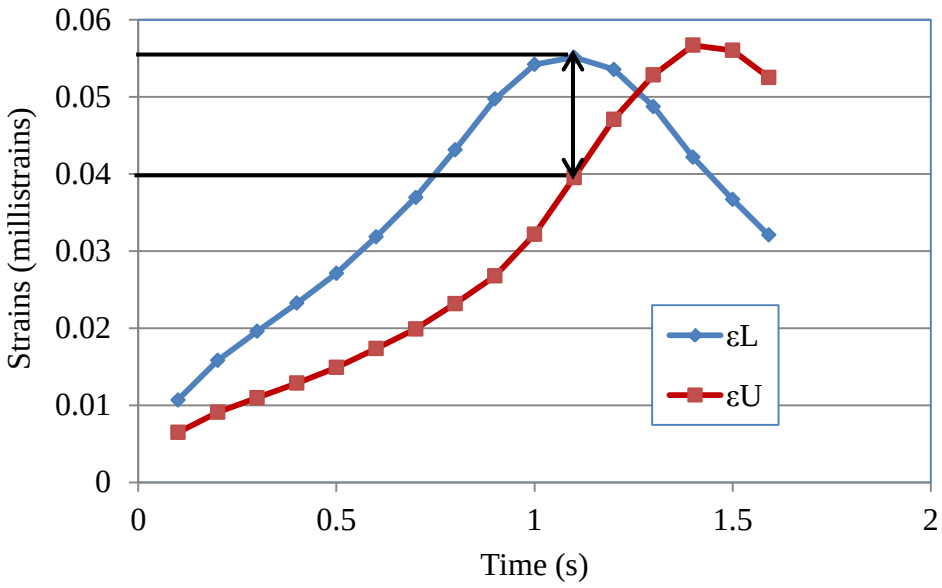

Figure 24: Loaded and unloaded strain profiles for moving aircraft

The dynamic LTE (S) is calculated using the peak ε_L value and the corresponding ε_U value at that instant. From Figure 24, the dynamic LTE (S) is calculated as follows:

$$LTE(S) = \frac{\varepsilon_U}{(\varepsilon_U + \varepsilon_L)} \tag{21}$$

$$LTE(S) = \frac{0.0395}{0.0395 + 0.0551} = 0.418$$

5.2.1 Effect of aircraft speed on critical tensile strain ($\varepsilon_{critical}$)

The 4-slab FEM model explained above was used to evaluate the effect of aircraft speed on pavement response. The slabs are loaded using a single wheel with tire pressure and footprint area similar to the NAPTV. The speed is varied from 0 fps (static case) to 20 fps. Spring constant of $2.1X10^7$ lbf/ft. is used for this analysis and the pavement damping is varied by

varying β from 0.2 s to 0.6 s. As the wheel travels across the joint, the critical tensile strain at the bottom of PCC layer is recorded. The critical tensile strain ($\varepsilon_{critical}$) values decrease with increase in the speed of the aircraft. The critical tensile strain values drop by 55%, 68% and 75% for β value of 0.2 s, 0.4 s and 0.6 s respectively as the speed increases from 0 fps to 20 fps. Lower $\varepsilon_{critical}$ values are obtained for higher β value (Figure 25).

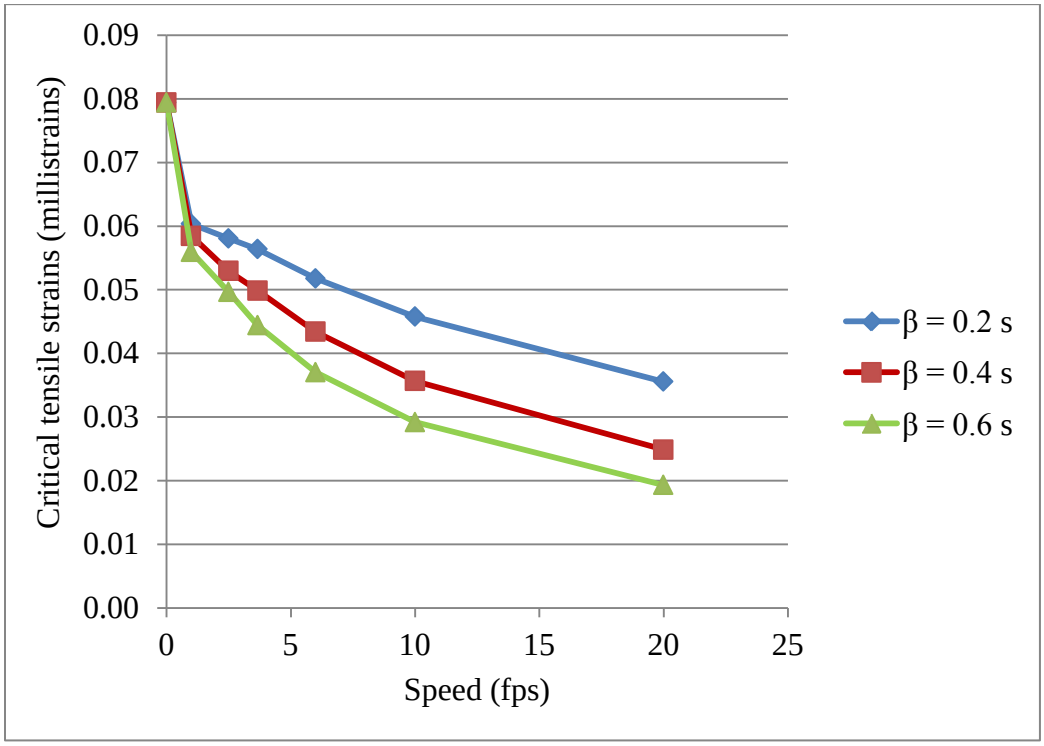

Figure 25: Effect of aircraft speed on critical strain values

5.2.2 Effect of aircraft speed on LTE (S)

Stress-based dynamic LTE is calculated under varying aircraft speeds using the responses obtained from FEM analysis for the MRC section. An aircraft with single wheel configuration is

used with the tire pressure of 210 psi and a total load of 55,000 lbs. The joint stiffness (k_s = 2.1X10^7 lbf/ft) is kept constant throughout the analysis. The speed of the aircraft and stiffness proportional damping factor (β) is varied. The results are plotted in Figure 26.

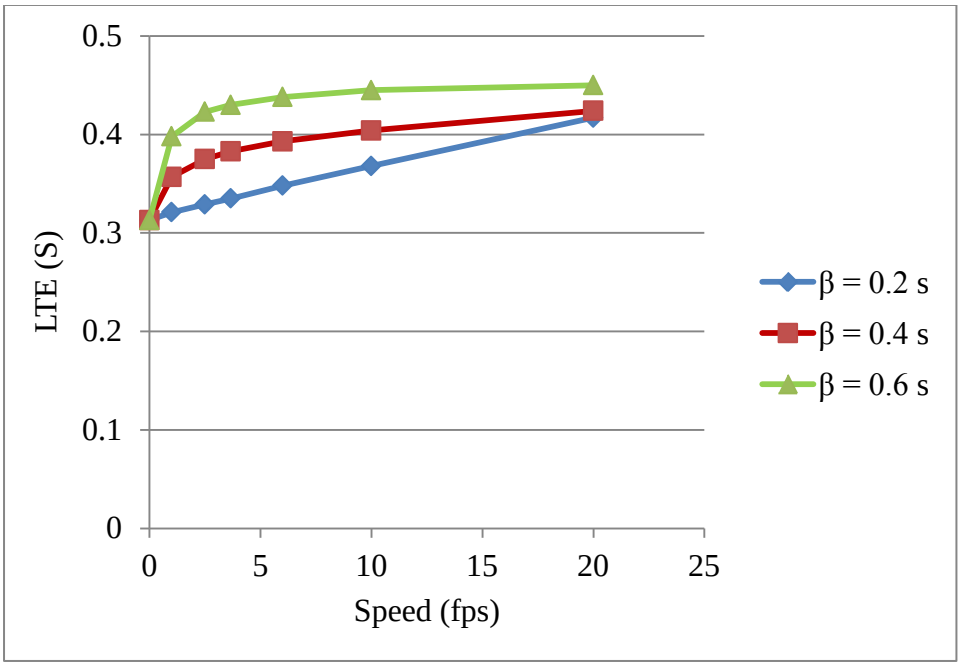

Figure 26: Effect of aircraft speed on LTE (S)

The analysis shows that dynamic LTE (S) varies with speed of the aircraft. A higher value of LTE (S) is obtained for higher speeds. As seen from the figure, for β = 0.2s, the LTE (S) value increases by 0.1 as the speed of the aircraft increases from 0 fps to 20 fps in a linear fashion. It is observed that the speed of the aircraft as well as the pavement damping value has an influence on LTE (S). These findings are consistent with previous studies (Yu et. al., 2010) which state that LTE (S) is higher under dynamic loads than static loads.

5.2.3 Effect of pavement damping on LTE (S)

The above findings called for the study of sensitivity of dynamic LTE (S) to pavement damping. The analysis is conducted using an aircraft with a single wheel configuration and a constant speed of 20 fps. The simplest aircraft configuration is used for the analysis to improve accuracy and save computational time. The pavement damping is varied by changing 'β' from 0.0 s to 0.6 s. For higher speeds and higher pavement damping values the LTE (S) values are closer to 0.5 which is the theoretical maximum value (Figure 27). Hence, this analysis is carried out for different values of joint stiffness by varying the spring constant from $2.1X10^8$ to $2.1X10^6$ lbf/ft.

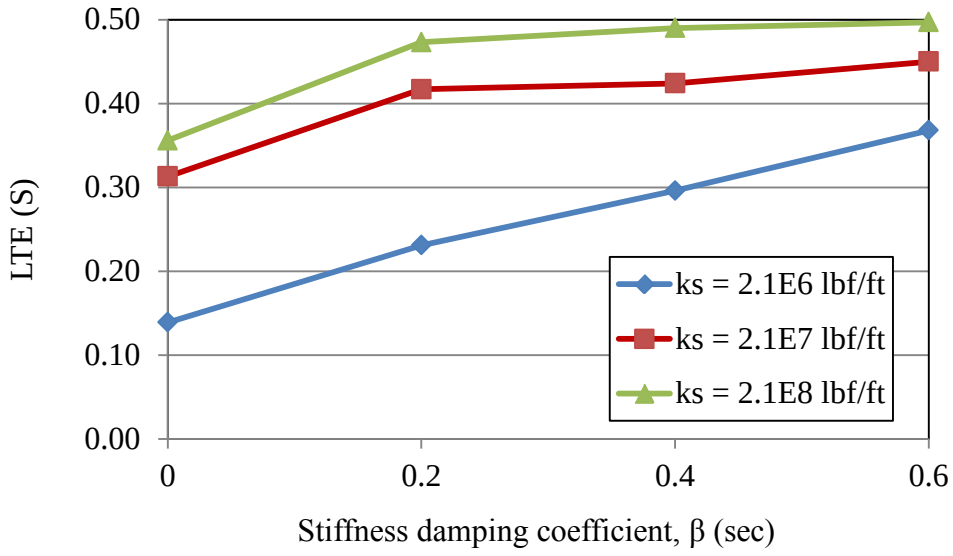

Figure 27: Effect of pavement damping on LTE (S)

The dynamic LTE (S) of the pavement system increases as the pavement damping value increases. The LTE(S) is more sensitive to joint stiffness at lower damping coefficient. On the

other hand, it is observed that dynamic LTE (S) at the joint is significantly affected by pavement damping at lower joint stiffness values.

5.2.4 Effect of aircraft wheel configuration on LTE (S)

The single wheel loading configuration was expanded to dual wheel configuration and dual tandem wheel configuration to study the effect of variation in aircraft load and wheel configuration on dynamic LTE (S). The analysis was carried out using a constant 'β' of 0.4 s, 'k_s' of 2.1X10^7 lbf/ft. and aircraft speed of 20 fps. The tire pressure of the wheels is varied for different wheel configurations to keep a fixed total load of 55,200 lbf on the pavement. The results are plotted in Figure 28.

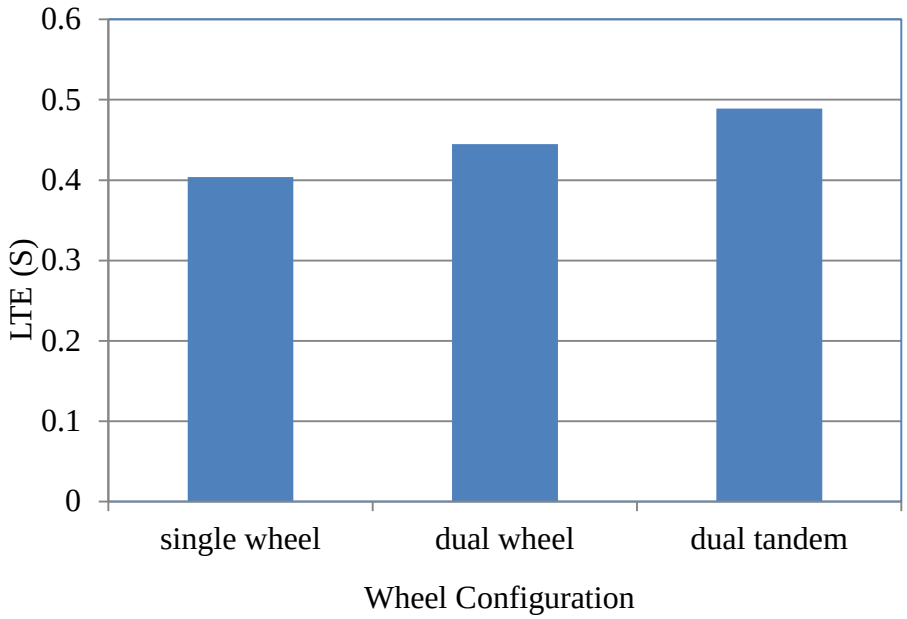

Figure 28: Effect of wheel configuration on LTE (S)

The results show that the dynamic LTE (S) increases by 10% as the wheel configuration changes from single wheel to dual wheel configuration and from dual wheel to dual tandem wheel configuration. This increase in LTE (S) may be due to increase in the number of loaded areas with the number of wheels. As the number of wheels increase, the number of loaded areas increase and more forces are transferred to the unloaded slab thus increasing the LTE (S).

5.3 Discussion

The pavement system is considered as a combination of three pure components for analysis: stiffness component, mass component and damping component. As mentioned in section 2.3 (equation 7), the external force $p(t)$ acting on the pavement due to traffic loading can be distributed as:

$$\mathbf{p(t) = f_S + f_I + f_D} \tag{22}$$

5.3.1 Effect of 'β' on critical tensile strains ($\varepsilon_{critical}$)

In section 5.2.1, it is observed that higher values of stiffness proportional pavement damping coefficient (β) yield lower critical strain values for a given aircraft speed. An increase in β value increases the damping force ($f_D = c\dot{u}$) in the pavement. Since the total external force acting on the pavement, $p(t)$, is constant for a given speed, the forces attributed to f_I and f_s are lower therefore causing lower critical strain values.

5.3.2 Effect of aircraft speed on critical tensile strains ($\varepsilon_{critical}$)

In section 5.2.1, it is observed that higher aircraft speeds yield lower critical strain values for a given β value. The damping force in the pavement system increases with the velocity of the

aircraft. An increase in damping force causes the critical tensile strains to decrease at higher velocity. Since damping forces are predominant, the mechanical responses are greatly influenced by the β values. On the other hand, at extremely low aircraft velocities ($\dot{u} \approx 0$), the damping forces are negligible ($f_D = 0$) and hence the strain values are maximum and tend to converge for different β values. This makes sense, because, at zero speed, the damping coefficient has no influence on mechanical pavement responses.

5.3.3 Effect of aircraft speed on LTE (S)

In section 5.2.2, it is observed that LTE (S) is sensitive to the speed of aircraft and increases with the speed of the aircraft. To understand this phenomenon, two different cases are stated below.

Case 1 is a hypothetical case wherein, at any given speed and 'β' value, the damping force in the loaded and unloaded slabs is similar. Case 2 is a realistic case wherein, at any given speed and 'β' value, the damping force in the loaded and unloaded slab is not similar.

Case 1: Figure 29 shows a schematic plot of aircraft speed versus critical tensile strain values ($\varepsilon_{critical}$) induced in the loaded and unloaded slabs under aircraft loading.

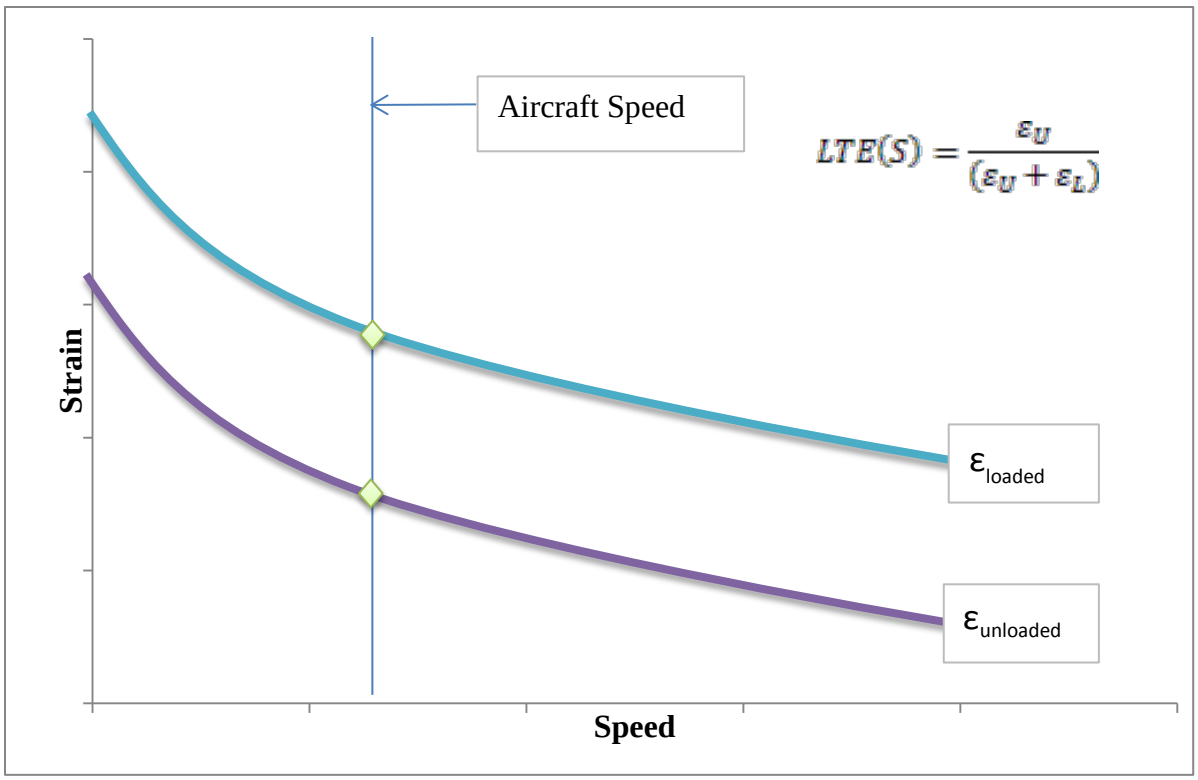

Figure 29: Effect of aircraft speed on LTE (S) (Case 1)

In this case it is assumed that the damping force induced in both the loaded and unloaded slabs is same for a given speed and given 'β' value. Since both the slabs experience same amount of damping force, the loaded strain (ε_L) and the unloaded strain (ε_U) profiles are parallel. Hence in this case, the LTE (S) would remain constant irrespective of the speed of the aircraft.

Case 2: A schematic plot of aircraft speed versus critical tensile strain values for loaded and unloaded slab is shown in Figure 30.

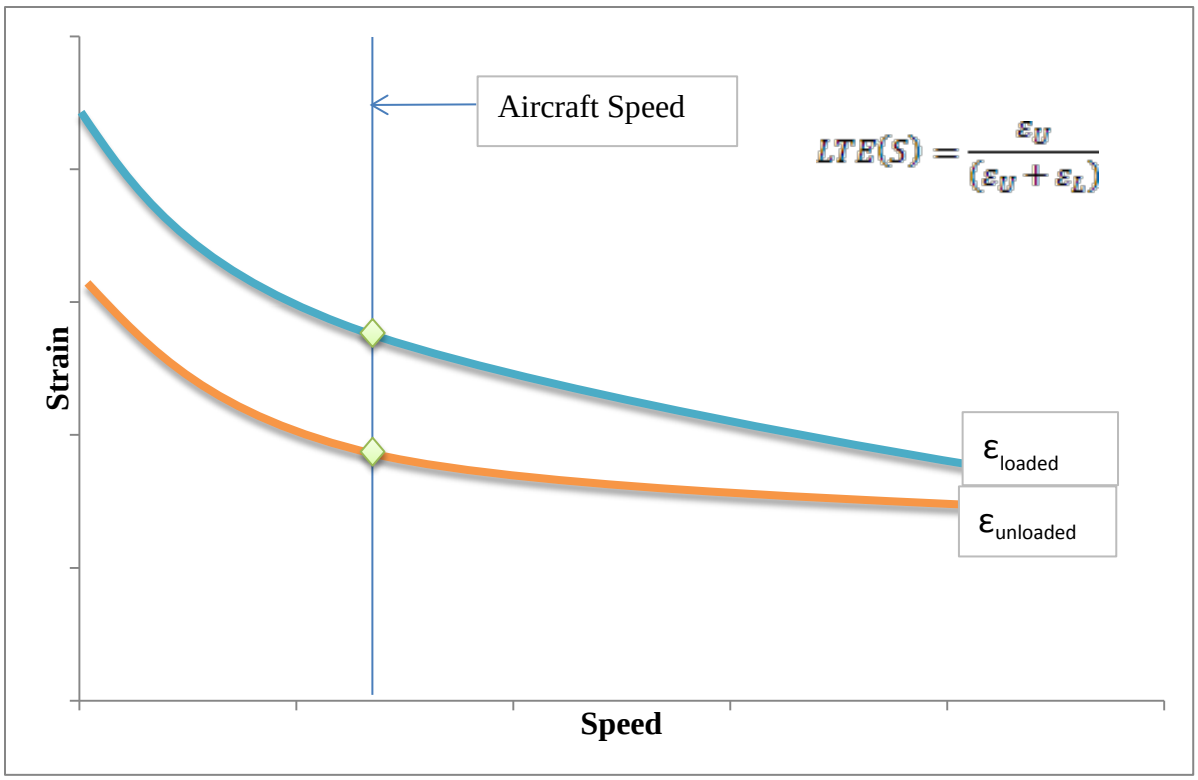

Figure 30: Effect of aircraft speed on LTE (S) (Case 2)

In this case, the damping force in the unloaded slab is lower than that in the loaded slab. The lower damping force in the unloaded slab may be because the unloaded slab could be experiencing the loads at lower speed than the actual aircraft speed. The lower damping force in unloaded slab will cause the unloaded strains to be higher than Case1. For case 2, ε_U values decrease at a slower rate than ε_L values as the speed increases. Therefore, the ε_L and ε_U curves are not parallel. An increase in aircraft speed results in higher LTE (S) values and at very high aircraft speeds the LTE (S) will reach 0.5 which is the theoretical maximum value. At extremely high aircraft speeds, damping force approaches infinity while the difference between ε_L and ε_U strain value approaches zero.

5.4 Summary

A 3D finite element program, ABAQUS (version 6.10), is used to model MRC rigid pavement test section to obtain pavement responses under dynamic aircraft loads. The ABAQUS model is calibrated using available HWD test data and dynamic full scale test data from strain gages embedded in MRC slabs. The two unknown parameters: joint stiffness of the dowel joints and concrete pavement damping are determined using the available field data. The calibrated ABAQUS model is then used to determine the dynamic responses of the test pavement under varying aircraft speeds. The sensitivity of LTE (S) to pavement damping, aircraft speed, aircraft load and wheel configuration is studied.

Chapter 6

Summary of findings, conclusions and recommendations

The research study examined the effect of pavement layer properties, loading characteristics and temperature curling on stress-based load transfer efficiency. The sensitivity of stress-based LTE to PCC layer modulus, base layer modulus, aircraft wheel configuration, and temperature gradient was studied under static loading conditions. A 3D finite element program, ABAQUS, is used to analyze the rigid pavement responses under dynamic aircraft loads. The ABAQUS model is calibrated using the available field HWD data and the strain gage data obtained from the NAPTF database. The sensitivity of LTE (S) to speed of moving aircraft and pavement damping is studied. The findings on the study and recommendations for future testing at FAA's NAPTF are listed in this chapter.

6.1 Summary of findings

The findings from the above analysis are summarized below:

1) Analysis of field strain profiles for CC2 test item joints shows that the LTE (S) under moving loads is within a range of 40% to 56%.
2) The LTE (S) under static loading conditions is insensitive to modulus of base layer and the PCC modulus.
3) Under static loading conditions, the LTE (S) increases by about 13% as the wheel configuration changes from single wheel to dual wheel, about 16% as the wheel configuration changes from single wheel to dual tandem and about 6% as the wheel configuration changes from single wheel to 3 duals in tandem (6-wheel).

4) The sensitivity of joint stresses to temperature gradient depends on the initial load on the slab. At 50 kips load, the joint stresses in MRG, MRC and MRS sections increase by 168.2 psi, 169.2 psi and 180.2 psi respectively, when the temperature gradient is reduced from 1 ^{o}F/in. to -1^{o}F/in.
5) For a 50 kips load and 0^{o}F/in. gradient, the LTE (S) for all the three sections was 0.34 which is much higher than the assumed 0.25 value.
6) For a 50 kips single wheel edge load, the LTE (S) value increases by about 0.04 with unit decrease in the temperature gradient. It is observed that stronger sub-structure yields larger variation in LTE (S) under changing temperature gradient.
7) The stiffness proportional pavement damping 'β' value for MRC section of CC2 test pavement is within a range of 0.15 to 0.4 s.
8) The critical tensile strain values drop by 55%, 68% and 75% for β value of 0.2 s, 0.4 s and 0.6 s respectively as the speed increases from 0 fps to 20 fps.
9) The dynamic LTE (S) at the joint increases with increase in the aircraft speed. As the speed increases from 0 fps to 20 fps, the LTE (S) value increases by 36%, 30% and 27% for 'β' values of 0.6s, 0.4s and 0.2s, respectively.
10) The LTE (S) value increases by 0.10 as the stiffness proportional damping coefficient from 0 to 0.2 s.
11) A change in wheel configuration from single wheel to dual wheel and from dual wheel to 4-dual tandem wheel causes the LTE (S) to increase by 10% at the speed of 20 fps.

6.2 Conclusions

The conclusions from the above analysis are summarized below:

1) The field LTE (S) values for CC2 test items under NAPTV loading are considerably higher than 0.25.
2) Temperature curling has a considerable effect on stresses at the joint and LTE (S) of the pavement. Positive temperature gradients yield lower joint stresses and lower LTE (S) than negative temperature gradients.
3) A stiffer sub-structure appears to cause lower stresses on either side of the joint as compared to a weaker sub-structure. However, they will have a similar LTE (S) value at a given temperature gradient. The LTE (S) at the joint appears to be insensitive to the sub-structure material properties and thicknesses.
4) The LTE (S) at the joint may reduce considerably at positive temperature gradients. The pavement life may be affected if the LTE (S) drops below the design value of 0.25.
5) Fairly accurate rigid pavement dynamic responses under moving aircraft can be obtained using 3D FEA if the damping parameters are known.
6) The critical tensile strain ($\varepsilon_{critical}$) values at the joint reduce significantly with increase in the speed of the aircraft.
7) The dynamic LTE (S) at the joint increases with aircraft speed and pavement damping value. The LTE (S) is more sensitive to pavement damping at lower aircraft speeds.
8) The dynamic LTE (S) at the joint is insensitive to the total load acting on the pavement but sensitive to aircraft wheel configuration.

6.3 Recommendations

The recommendations for future work are based on the findings and conclusions of this research analysis. These include:

1) The field LTE (S) values for doweled PCC slabs under moving aircraft loads for CC6 test pavement and other airports can be determined to verify if the dynamic LTE (S) is greater than 0.25.
2) A typical range of variation in the temperature gradients at airports in extreme climatic regions can be determined. The variation in critical stresses and the load transfer efficiency at the joints due to these temperature gradients can be analyzed.
3) In this research, the sensitivity analysis for LTE (S) is mainly carried out using a single wheel and dual tandem wheel configuration. This analysis can be expanded to more complex aircraft gear configurations.
4) The pavement damping values may vary with pavement layer materials properties, configuration, loading and other factors. Further research is necessary to analyze the sensitivity of pavement damping to these factors.
5) In this research, a linear elastic finite element model is developed using ABAQUS to obtain pavement responses under dynamic loading. A more realistic non-linear damage model with inclusion of cracks can be developed to analyze pavement responses and eliminate the error in measured (field) and calculated responses.
6) This research was limited to evaluation of doweled joints in rigid pavements. The effect of other load transfer mechanisms / types of joints on rigid pavement design can be evaluated.

List of References

ABAQUS/CAE User's Manual – Version 6.10. Dassault Systems Simulia Corp., Providence, RI, USA, 2010

American Association of State Highway and Transportation Officials. "The AASHO Road Test". Report 5, Special Report 61E, Washington D. C., 1962.

A. Wadkar. "Study of load transfer efficiency of airfield rigid pavement joints based on stresses and deflections". M.S. Thesis, Dept. of Civil & Environ. Eng., Rowan University., NJ, 2010

Brill, D., and E. Guo. "Analysis of In-Pavement Sensor Data for CC2 New Rigid Test Items at the FAA national Airport Pavement Test Facility". Eighth International Conference on Bearing Capacity of Roads, Railways and Airfields, UIUC, 2009.

Brill, D. R., I. Kawa, and G. F. Hayhoe. "Development of FAARFIELD airport pavement design software". Transportation Systems Workshop, 2004.

Brill, D. R., G. F. Hayhoe, and L. Ricalde. "Analysis of CC2 Rigid Pavement Test Data from the FAA's National Airport Pavement Test Facility". Proceedings of the Bearing Capacity of Roads Railways and Airfield (BCRRA) Conference, Trondheim, Norway, June 2005

Chatti, K., J. Lysmer, and C.L. Monismith. "Dynamic Finite-Element Analysis of Jointed Concrete Pavements". *Transportation Research Record* 1449, National Research Council, Washington, D.C., 1994, pp. 79-90.

Chatti, K., Y. G. Ji., and R. S. Harichandran. "Dynamic Time Domain Back-calculation of Layer Complex Moduli and Thicknesses in Asphalt Concrete Pavements". CD-ROM. *Transportation Research Board*, National Research Council, Washington, D.C., 2004.

Chopra, A. K. *Dynamics of Structures – Theory and applications to Earthquake Engineering.* Prentice Hall. 3rd edition. 2007.

Darter, M.I., K.T. Hall, and C. Kuo. "Support under Portland Cement Concrete Pavements". NCHRP Report 372. Washington, DC: National Cooperative Highway Research Program. 1995.

Daiutolo, H. "Control of Slab Curling in Rigid Pavements at the FAA National Airport Pavement Test Facility". Proceedings of the Accelerated Pavement Testing (APT), Third International Conference, Madrid, Spain, 2008.

Federal Highway Administration. "Evaluation of Joint and Crack Load Transfer Final Report". 2003.

Fanous, F., D. Shannon. "Field and analytical investigations of dowel performance in transverse joint of concrete pavement". Proceedings of the 2008 Mid-Continent Transportation Research Forum, Madison, Wisconsin, August 2008.

Federal Aviation Administration, NAPTF database CC2 (2010), Retrieved from http://www.airporttech.tc.faa.gov/NAPTF/. [December 2010]

Federal Aviation Administration, Office of Airport Safety and Standards. "Standards for Airport Pavement Design and Evaluation". Advisory Circular 150/5320-6D, 1995.

Federal Aviation Administration. "Airport Pavement Design and Evaluation". Advisory Circular 150/5320-6E, 2009.

Garg, N., E. Guo, and R. McQueen. "Operational Life of Airport Pavements". Publication DOT/FAA/AR-04/46, USDOT, FAA, 2004.

Guo, E.H., J.A. Sherwood and M.B Snyder. "Component Dowel Bar Model for Load Transfer Systems in PCC Pavements". *Journal of Transportation Engineering*, Vol.121, No.3, 1995. pp. 289-298.

Guo, E. H. "Back Estimation of Slab Curling and Joint Stiffness". International conference on pavements, Florida, USA, 2001.

Hammons, M. I., D. W. Pittman, and D. D. Mathews. "Effectiveness of Load Transfer Devices". Publication DOT/FAA/AR-95/80. FAA, U.S. Department of Transportation, 1995.

Huang, Y., and S. T. Wang. "Finite Element Analysis of Concrete slabs and its implications for Rigid Pavement Design". *Highway Research Board*, No. 466, 1973, pp. 55-69.

Huang, Y. H. *Pavement Analysis and Design*. Pearson Education, Inc., Upper Saddle River, NJ, 2004.

Hughes, Thomas J. R. *The Finite Element Method: linear static and dynamic finite element analysis*. Prentice Hall, Englewood Cliffs, NJ, 1987.

Ioannides, A. M., M. R. Thompson, and E. J. Barenberg. "Finite Element Analysis of Slabs-On-Grade using a Variety of Support Models". Proceedings, Third International Conference on Concrete Pavement Design and Rehabilitation, Purdue University, W. Lafayette, 1985.

Kawa, I., D. R. Brill, and G. F. Hayhoe. *FAARFIELD* – "New Airport Thickness Design Software". FAA Worldwide Technology Transfer Conference. Atlantic City, NJ, USA, 2007.

Khaki, A. M., and E. Azadravesh, "Generating a 3D model for evaluating the joint opening effects on load transfer efficiency in concrete pavements, using ABAQUS". 5th National Congress on Civil Engineering, Ferdowsi University of Mashhad, Mashhad, Iran, 2010.

Masad E., Taha R. and Muhunthan B., "Finite-Element Analysis of Temperature Effects on Plain-Jointed Concrete Pavements". *Journal of Transportation Engineering*, Vol. 122, No. 5, 1996, pp. 388-398.

M. Kim. “Three dimensional finite element analysis of flexible pavements considering non-linear pavement foundation behavior”. Ph.D. dissertation, Dept. Civil Eng., Univ. of Illinois at Urbana-Champaign, IL, 2005

Ricalde, L., and H. Diautolo (2004). “New Rigid Pavement Construction and Testing At the FAA National Airport Pavement Test Facility (NAPTF)”. Federal Aviation Administration. http://www.airporttech.tc.faa.gov/naptf/Downloads/CC2%20Test%20Items%20ICPT05.pdf, [January 2011].

Rijlaarsdam, D. J. “Modeling damping in linear dynamic systems”. Final Bachelor Project. DCT report number : DCT 2005.39, 2005

Smith, K. D., and J. R. Roesler. “Review of fatigue models for concrete airfield pavement design”. ASCE Airfield Pavement Specialty Conference, Las Vegas, NV, 2003.

Timoshenko, S. *Theory of elastic stability*. 2nd edition. McGraw-Hill, New York 1961.

T. Wei. “Response Modeling of Pavement subjected to Dynamic surface loading based on stress-based multi-layered plate”. Ph.D. dissertation, Dept. Civil Eng., Ohio State Univ., OH, 2007

Wadkar, A., A. Zapata and L. Musumeci. “Analysis and Evaluation of Load Transfer Efficiency of Rigid Airfield Pavements”. Presentation in Data Analysis Working Group Forum, TRB, 2010.

Wadkar, A., A. Norton, C. Tomlinson, A. Zapata, L. Musumeci, E. H. Guo, D. B. Cleary, Y. A. Mehta. “Load Transfer Efficiencies of Rigid Airfield Pavement Joints Based on Stresses and Deflections”. *Transportation Research Board* 89th Annual Meeting, 2010.

WSDOT Pavement Guide, “Pavement Types”
http://training.ce.washington.edu/wsdot/modules/02_pavement_types/ [January 2011]

Westergaard, H.M. “Stresses in Concrete Pavements Computed by Theoretical Analysis”. Public Roads, Vol. 7, 1926a, pp. 25-35.

Westergaard, H.M. “Analysis of Stresses in Concrete Pavement Due to Variations of Temperature”. *Proceedings, Highway Research Board*, Vol. 6, 1926b, pp. 201-215.

Yu, X., Y. Zhou, J. Peng, Z. Tan, and E. Guo. “Joint Load Transfer Efficiency of Rigid Pavement Considering Dynamic Effects under a Single Moving Load”. FAA Worldwide Technology Transfer Conference. (CD-ROM), Atlantic City, NJ, USA, 2010.

Zaghloul S. and T. D. White. “Guidelines for Permitting Overloads. Part 1. Effect of Overloaded Vehicles on the Indiana Highway Network”. Research Report FHWA/IN/JHRP-93/5, FHWA, U.S. Department of Transportation. 1994.

Zidri, M., N. Abraik., J. Neil., and M. Ben Ouezdou. “Modeling of the Stresses and Strains Distribution in an RCC Pavement Using the Computer Code Abaqus". *Electronic Journal of Structural Engineering*. 2009.

Bibliography

Channakeshava, C., F. Barzegar, and G. Voyiadjis. “Nonlinear FE Analysis of Plain Concrete Pavement with Doweled Joints”. *Journal of Transportation Engineering*, ASCE, Vol. 119, No. 5, pp. 763-781, 1993.

Gillespie, T. D., S. M. Karamlhas, D. Cebon, M. W. Sayers, M. A. Nasim, W. Hansen and N. Ehsan. “Effects of heavy vehicle characteristics on pavement response and performance”. Final Report for NCHRP. USA. 1993.

Pickett, G. and G. Ray. “Influence Charts for Rigid Pavements”. Transactions, American Society of Civil Engineers (ASCE), Vol. 116, pp. 49-73, 1951.

Salsilli, R. A., E. J. Barenberg and M. I. Darter. “Calibrated Mechanistic Design Procedure to Prevent Transverse Cracking of Jointed Plain Concrete Pavements”. Proceedings of the fifth International Conference on Concrete Pavement Design and Rehabilitation, Purdue University. West Lafayette, IN, pp. 71-90, 1993.

US Army Corps of Engineers. “Lockbourne No. 1 Test Track, Final Report”. Rigid Pavement Laboratory, 1946.

Wang, S.K., M. Sargious and Y.K. Cheung, “Advanced Analysis of Rigid Pavements”. *Transportation Engineering Journal*, ASCE, 98(TE1): pp. 37-44, 1972.